FABRICATION of BONE SURFACE MIMICKED BIODEGRADABLE CHITOSAN-GRAPHENE OXIDE NANOCOMPOSITE MEMBRANES

by

Fatih Puza

B.Sc, Bioengineering, Yildiz Technical University, 2009

Submitted to the Institute of Biomedical Engineering
in partial fulfillment of the requirements
for the degree of
Master of Science
in
Biomedical Engineering

Boğaziçi University
2017

FABRICATION of BONE SURFACE MIMICKED BIODEGRADABLE CHITOSAN-GRAPHENE OXIDE NANOCOMPOSITE MEMBRANES

APPROVED BY:

Assoc. Prof. Dr. Bora Garipcan .....
(Thesis Advisor)

Assist. Prof. Dr. Duygu Ege .....

Assist. Prof. Dr. Sedat Odabaş .....

DATE OF APPROVAL: 09 January 2017

ACKNOWLEDGMENTS

I would first like to express my deep gratitude to Assoc. Prof. Dr. Bora Garipcan, who expertly supervised me during my thesis and also inspired me for my future academic career. It was an honor and pleasure to work with him.

I would like to thank my committee members, Assist. Prof. Dr. Duygu Ege and Assist. Prof. Dr. Sedat Odabaş, for their contributions and positive comments about my thesis.

My deepest gratitude goes to my family, who have always encouraged and supported me throughout my life. Also, I would like to thank to Sevde Üçpınar for motivating me during my research and her endless support. This thesis would not be completed without their support.

I would like to extend my great appreciation to my teammate, Sabra Rostami, and other members of Bioscubus Laboratory for their helps. For their contributions to my thesis, I would like to thank Zeiss for Confocal Microscopy analysis. In addition, I am grateful to Renishaw, which provided Raman Spectroscopy analysis.

ACADEMIC ETHICS AND INTEGRITY STATEMENT

I, Fatih Puza, hereby certify that I am aware of the Academic Ethics and Integrity Policy issued by the Council of Higher Education (YÖK) and I fully acknowledge all the consequences due to its violation by plagiarism or any other way.

Name :

Signature:

Date:

ABSTRACT

FABRICATION of BONE SURFACE MIMICKED BIODEGRADABLE CHITOSAN-GRAPHENE OXIDE NANOCOMPOSITE MEMBRANES

Biomaterials and tissue engineering applications are promising to heal defected bone tissue. Direct interaction of cell and biomaterial surface occurs and surface properties are able to change cellular responses. In this thesis, it was aimed to fabricate chitosan (CH) and graphene oxide (GO) based biodegradable membranes, which are able to mimic natural bone surface topography. Micro and nanostructures of bone surface was copied by soft lithography technique with using polydimethylsiloxane(PDMS). Human osteoblast cells (hFOB 1.19) were used to evaluate effects of surface topography and GO addition. Surfaces were modified with hydroxyapatite (HA) nanoparticles to enhance osteoconductivity. Physical and chemical characterization of membranes was performed by scanning electron microscopy, confocal microscopy and spectroscopy techniques. SEM and confocal microscopy imaging of membranes showed that bone surface topography mimicked, successfully. Spectroscopy techniques, namely FT-IR, XPS, Raman and XRD demonstrated chemical compositions of CH, GO and HA modification. hFOB cell morphology was evaluated by using SEM at day 7. HA modification and bone surface mimicking provided more surface area, so that spread of cell was increased and surface of membranes covered with the cells. In addition, GO addition had positive impact on cell spreading when it is compared with pure CH. Cell viability was analyzed by performing MTT assay. The obtained results demonstrated that cell viability increased in bone surface mimicked membranes.

Keywords: Biomimetic, Bone Surface Mimicking, Human Osteoblast, Soft Lithography, Chitosan, Graphene Oxide, Hydroxyapatite.

ÖZET

KEMİK YÜZEYİNİ TAKLİT EDEN BİYOBOZUNUR KİTOSAN-GRAFEN OKSİT MEMBRANLARIN ÜRETİMİ

Biyomalzeme ve doku mühendisliği uygulamaları, hasar görmüş kemik dokusunu iyileştirmek için umut vaadetmektedir. Biyomalzeme ve hücreler arasında direk etkileşim oluşmaktadır ve yüzey özellikleri hücre yanıtlarını değiştirme yeteneğine sahiptir. Bu tezde, kitosan ve grafen oksit kullanarak biyobozunur, kemik yüzey topografisini taklit etme yeteneğine sahip membranların üretilmesi hedeflenmiştir. Kemik yüzeyindeki mikro ve nanoyapılar, polidimetilsiloksan (PDMS) ve yumuşak litografi kullanılarak kopyalanmıştır. İnsan kemik hücresi (hFOB 1.19), yüzey topografi ve grafen oksit etkisini değerlendirmek için kullanılmıştır. Osteokonduktifliği arttırmak için yüzeyler nanopartikül hidroksiapatit (HA) ile modifiye edilmiştir. Membranların fiziksel ve kimyasal karakterizasyonları, taramalı elektron mikroskobu, eşodaklı mikroskop ve spektroskopi teknikleri ile gerçekleştirilmiştir. Kemik yüzey topografisinin başarı ile taklit edildiği taramalı elektron mikroskobu (SEM) ve eşodaklımikroskop ile görülmüştür. CH, GO membranlarının ve HA modifikasyonlarının kimyasal içerikleri FT-IR, XPS, Raman ve XRD spektroskopi teknikleri ile elde edilmiştir. hFOB hücre morfolojisi 7. günde SEM kullanılarak görüntülenmiştir. HA modifikasyonunun ve kemik yüzey taklidinin daha fazla yüzey alanı yaratması sebebiyle, hücre yayılmasının arttığı ve yüzeylerin hücreler ile kaplandığı gözlemlenmiştir. Bunlara ek olarak, normal CH ile karşılaştırıldığında GO ekleme hücre yayılımında olumlu etki yaratmıştır. Hücre canlılığı MTT testi gerçekleştirilerek analiz edilmiştir. Elde edilen sonuçlar, hücre canlılığının kemik yüzey taklidi membranlarda arttığını göstermiştir.

Anahtar Sözcükler: Biyomimetik, Kemik Yüzey Taklidi, İnsan Kemik Hücresi, Yumuşak Litografi, Kitosan, Grafen Oksit, Hidroksiapatit.

TABLE OF CONTENTS

LIST OF FIGURES

LIST OF TABLES

LIST OF ABBREVIATIONS

CH	Chitosan
GO	Graphene Oxide
HA	Hydroxyapatite
BSM	Bone Surface Mimicked
PDMS	Polydimethylsiloxane
hFOB	Human Fetal Osteoblast
SEM	Scanning Electron Microscope
FT-IR	Fourier Transform Infrared Spectroscopy
XPS	X-ray Photoelectron Spectroscopy
XRD	X-ray Diffraction Spectroscopy
PBS	Phosphate Buffered Saline
MTT	(3-(4,5-Dimethylthiazol-2-yl)-2,5-Diphenyltetrazolium Bromide)
DMSO	Dimethyl Sulfoxide

1. INTRODUCTION

1.1 Motivation

Bone tissue plays key roles in body and has different responsibilities. The first is mechanical strength, which is vital for covering and protecting organs that have essential activities to regulate whole body. For instance, brain is protected by skull that is made from bone tissue. Furthermore, inner side of bone is bone marrow, which reserves stem cells and produces immune cells. The other importance of bone tissue is mineral concentration balancing of body. In the structure of bone tissue, great amount of calcium and phosphate minerals are reserved. In addition to these, movement process is impossible without a healthy skeleton. Bone tissue provides junctions to muscles and they attach together to make movement possible [1].

Some diseases such as osteoporosis, osteogenesis imperfecta and osteoarthritis or injuries may lead defects in bone structure. In such cases, bone fractures and deformation is commonly observed and it causes immobility of patient. Various types of grafting methods are being used in clinical treatment, but sufficiency of such treatments are very limited [2]. Biomimetic and bone tissue engineering applications offers great potential to overcome bone structure related disorders, since designing various types of environments for regenerative bone cells is possible. In tissue engineering, the term of biomimetic describes mimicking natural extracellular matrix (ECM), where cells are located, with using biomaterials. Chemical and mechanical properties, such as stiffness and roughness of used biomaterials are able to alter cell responses and because of that it is significant to understand preferred environments of cells [3].

It is known that focal contacts of cells and microstructures on material surface can lead to change in cell conformation and mechanisms, as well [4].Some studies demonstrated that similar structure with natural bone topography enhanced stem cell differentiation, osteogenic marker expressions and osteoblast functions [5, 6]. On the

other hand, chemical interactions are vital for cell mechanisms regulation, as well. Chitosan (CH) is a promising material that has excellent biocompatibility, osteoconductivity [7]. Graphene oxide (GO) is a carbon based material with nanosize, which enhances cell interaction [8]. Furthermore, hydroxyapatite (HA) is the main component of bone tissue and contains preferred properties for bone tissue engineering [9].

Preferred biomaterials in this thesis enabled to mimic bone surface topography and offerred excellent chemical properties. Analyzing effect of bone surface topography with chemical properties of materials and deciding, which is more dominant may provide better understanding of cellular mechanisms and potential applications in bone tissue engineering.

1.2 Objectives

In this thesis, bone surface topography impact on human osteoblast (hFOB 1.19) was evaluated. For this aim, bone surface topography was mimicked with soft lithography technique by using polydimethylsiloxane (PDMS) and it was used as mold. Chitosan (CH) was chosen as main biomaterial to mimic bone surface topography. The obtained topography on PDMS surface was copied to CH surface with solvent casting process. Furthermore, graphene oxide (GO) added nanocomposite membranes were fabricated to analyze cell responses against GO. On the other hand, hydroxyapatite nanoparticles, which are abundant in bone tissue, modification was conducted to enhance cell viability and spread. The main objectives of this thesis were:

1. Mimicking surface topography of bone.
2. Fabrication of CH, CH/GO nanocomposite membranes and modification of HA on the membranes.
3. Characterization of physical and chemical properties.
4. Investigation of human osteoblast cell responses on the membranes.

1.3 Outline

This thesis is presented as follows: In chapter 2, background information about bone structure, bone tissue engineering and material choice were explained. In chapter 3, experimental procedures were explained. In chapter 4, the results were presented. In chapter 5, obtained results were interpreted.

2. BACKGROUND

2.1 Bone Formation and Remodeling Process

Bone is made from various materials, which construct composite structure. The composite structure provides unique biological and mechanical properties such as high strength and fracture resistance. Bone is constructed by different layers of several organic and inorganic molecules. Mainly, it consists of collagen matrix and hydroxyapatite (HA), which is nano-sized. HA conformation in the structure is formed and regulated by aligned fibril collagen matrix [10].

Bone formation is completed in a two-step process. The first step is primary osteogenesis and cartilage formation, which contains 10-20 nm in diameter collagen fibrils, is observed during the primary osteogenesis. Furthermore, matrix production and mineralization process activation occurs in this step. By the time, woven structure of bone is obtained with the help of rapid and irregular form of mineralization. The secondary osteogenesis is the step of remodeling. Woven bone form of primary step is remodeled to shape more effective tissue. After secondary step, parallel fibers and lamellar bone structure is observed. HA molecules are found in collagen matrix and formed to an optimal structure. Mineralization of collagen matrix results in providing remarkable mechanical properties to bone tissue. Ability of controlling mineralization process is significant for endless remodeling capacity since bone is a dynamic tissue [10]. Figure 2.1 shows the bone formation process [11].

2.2 Bone Matrix Minerilization

Bone is originated from various material types, which are minerals (50-70%), organic matrix (20-40%), water (5-10%) and lipids (3%). Most of mineral content is made by HA, but rare amount of magnesium, acidy phosphate and hydroxyl groups are

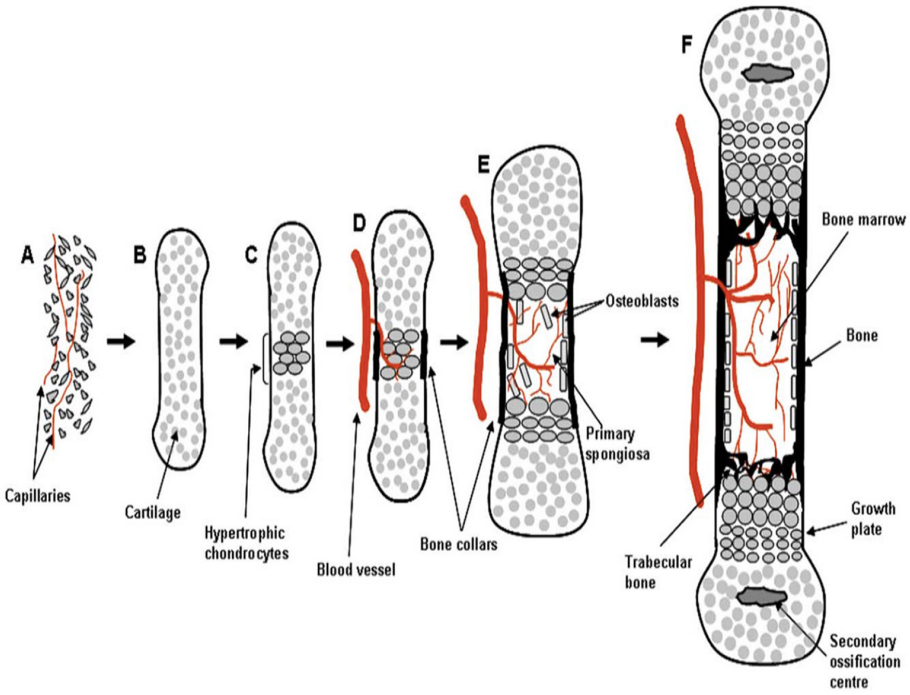

Figure 2.1 Bone formation scheme [11].

found in its structure. HA is a calcium phosphate based and crystal formed material. Matrix mineralization is essential for formation of bone and remodeling process. Different kinds of proteins, which are able to bind calcium and phosphate are produced and secreted during this step. With the help of these proteins, HA crystals are modeled. Mineral content of bone is responsible for mechanical rigidity and load-bearing. On the other hand, organic matrix is responsible for elasticity [3].

Mineralization process is a complex process and starts from the ends of collagen fibrils. Osteoblasts can synthesize matrix extracellular vesicles, which augments mineralization process. Calcium and phosphate amount goes up and it is beneficial for crystal formation. HA mineralization is not possible in absence of matrix extracellular vesicles since HA does not precipitate in body fluid. The vesicles are formed by nucleation core, which contains proteins, calcium, acidic phospholipids and phosphate. HA crystal production and growth increases when bone maturation continues. It was found that phoshoprotein kinases and alkaline phoshophatases indicates activity during bone mineralization [3].

2.3 Bone Disorders and Defects

Defects in the bone tissue structure lead to loss of significant functions namely, movement restrictions, absence of homeostasis and immunologic agents. Physical trauma and metabolic disturbances may cause disorders in bone tissue structure. Bone tissue is a dynamic tissue, which is modeled by deposition and resorption processes. Osteoblastic extracellular matrix generation is a formation process and then calcification of this matrix occurs during the deposition process. On the contrary, produced bone and calcified minerals are disposed during resorption. The resorption process is conducted by osteoclast cells. Equilibrium between bone formation and removal phenomena is vital to get healthy bone tissue. For instance, osteomalacia is a disorder, which makes bone softer. The main reason of this disorder is low degree of matrix calcification. In addition, osteoporosis is a common disorder among elder people. The strength of the bone decreases among the ages and bone breaking risk goes up. In this case, increase in osteoblastic or decrease in osteoblastic activation might lead to osteoporosis [12]. Figure 2.2 indicates bone formation process, which is regulated by osteoblast and osteoclast cells.

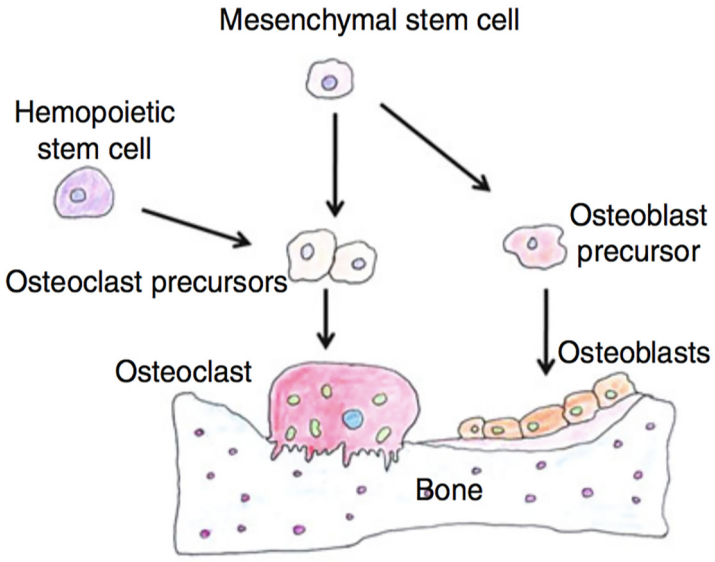

Figure 2.2 Bone formation by osteblast and osteoclast cells [13].

2.4 Clinical Approaches

Bone tissue is able to regenerate itself by the activation of osteoblast cells. However, large defects cannot be healed because of being regeneration capacity of bone is insufficient. In such cases, different treatment techniques are needed to be applied to heal defected bone tissue. Grafting techniques are beneficial methods and physicians perform different types of grafting methods to heal the defected tissue. Currently, autograft and allograft bone transplant is commonly used by physicians. Autologous tissue is obtained from patient itself and there is no risk of immunoreactions after the transplantation. The first drawback is a need of second surgery to gather healthy tissue from patient. Furthermore, the amount of healthy tissue might not be sufficient for each transplantation [14].

The other way of grafting is allograft, which transplanted tissue is gathered from other donors. The main advantage of this method is overcome of quantity restriction and various bone types can be obtained from other people. The disadvantage of allograft is immune system of the patient is activated because of foreign immune agents and this issue decreases success of transplantations. To overcome this problem, patients use specific immunosuppressive drugs to eliminate the rejection risk of bone graft. However, usage of such drugs enhances risk of infections or other diseases [14].

2.5 Bone Tissue Engineering Approaches

Tissue engineering is a multidisciplinary discipline, which combines biology, materials science and engineering approaches. Designing and fabrication of synthetic scaffolds, which are able to mimic extracellular matrix offers promising perspective and applications to overcome biological disorders and defects. These kinds of scaffolds have some advantages when they are compared with conventional clinical approaches. First of all, they offer reduce in disease risk, which might come from donor, immunoreactions and infection risk. Furthermore, great amount of biomaterials can be used for

designing artificial scaffolds and alterations of such materials gives chance to get better controlling of cell behavior [15]. Preferred properties of synthetic scaffolds for bone tissue engineering are indicated in Table 2.1 [15].

Table 2.1
Synthetic bone tissue scaffolds.

Properties of Synthetic Bone Tissue Scaffolds
Good mechanical strength
Porous structure
Osteoinduction
Integration with host tissue
Controllable degradation
Biocompatibility
Prevention of chronic immunoresponses

Two different strategies are extensively used in tissue engineering applications. The first strategy is that implantation of scaffolds and seeded cells together into the body, which provide ECM production in a controlled in-vitro environment. The second method is implantation of scaffolds without seeding cells as soon as possible after defect. In bone bone engineering, mature osteoblast cells and mesenchymal stem cells (MSC), which are capable to differentiate to osteoblast are used [15].

2.6 Mechanical Signals and Bone Tissue

Mechanical match between scaffold and surrounding tissue is very significant to increase success rate of applications. Signal mechanisms of cells are activated by mechanical cues of extracellular matrix and each cell types give different responses when they receive mechanical signals. Such signals are sensed by receptors, which are located on cell membrane and conducted inside the cell with the help of cytoskeleton. Mechanical signals can be stiffness, topography, shear stress and surface energy [16]. Surface of bone tissue is mostly constructed by HA molecules, which is a ceramic

material and tough. On the other hand, mechanical properties change with the location and function of bone since it is formed from diverse layers. When it is considered, defect region and bone type should be decided before applications [7].

Mechanical properties of scaffolds have enormous affect on biological processes such as adherence, differentiation and proliferation. Because of that, scaffolds should be designed with mechanical properties, which trigger osteoinductivity. In case of bone tissue engineering, load bearing property is quite affective to regulate cell responses since deformation of scaffold occurs during force applications. In addition, mechanical signals have influence on osteointegration since scaffold forms an interface with cells. Composite material fabrication is quite useful for arrangement of mechanical properties such as strength, elastic moduli, elongation and load bearing [7].

2.7 Mimicking of Bone Surface

Osteoblasts show sensitivity to surface roughness and chemistry. Focal contacts of cells and microstructures on material surface can lead to change in conformation of microfilaments, which are found inside cells. Also, signal transduction can be changed by integrin proteins, which are bound to cell membrane that results in gene transcription and protein synthesis when the topography is altered. If surface is rough, cells can make focal attachments between surface peaks. On the other hand, smooth surface has different influence on cell behavior. In this case, cells tend to spread [4].

The outer layer of bone is called periosteum, which plays key roles for bone repair and regeneration. Stem cells are found under the layer of periosteum, and they are activated when bone is injured. Underneath the periosteum, there is a unique topography that is shaped from micro and nanostructures. It was demonstrated that this unique topography has ability to regulate cell functions [5]. Bone surface contains nano-sized molecules such as collagen and HA, which make bone surface rough. It has been proved that surface roughness has influence on cell behavior. For this reason, mimicking of surface roughness provides benefits on regulation of cell mech-

anisms. Researchers has paid attention to mimic surface structures while they are designing materials for orthopedic applications since material surface forms an interface with natural tissue. Various methods namely chemical etching, anodization and addition of nanoparticles are used for creating nanostructures of bone surface. Shi et al. fabricated micropatterned poly(dimethylsiloxane) (PDMS) substrates, which mimic microstructure of bone topography. Then, PLGA biopolymer was spincoated to copy micropatterns from PDMS surface and gathered nanosheets of PLGA. Stem cells differentiation was evaluated and concluded that surface mimicking leads to increase of osteogenic markers and gene expressions [5]. Palin et. al. created similar nanostructures on titania and used PLGA to design a scaffold for osteoblasts. They observed that mimicked surface enhanced osteoblast functions [6].

Furthermore, chemical and physical structure of bone surface has been mimicked in various studies. In another work, polycaprolactone (PCL) scaffolds were designed with nanorough surface via biphasic calcium phosphates and nano-HA. Osteogenic differentiation of adipose tissue-derived mesenchchymal stem cells were evaluated and it was indicated that scaffolds with nano-roughness triggered much osteogenic gene expression [17].

2.8 Soft Lithography

Soft lithography is a micro engineering technique, which gives opportunity to replicate surface structures. Surfaces structures, which can range from 30 nm to 100 μm are copied by elastomeric stamp. Soft lithography is a cost efficient and quite effective to produce surface patterns for different applications and useful method to mimic surface topography [18].

Poly(dimethylsiloxane) (PDMS) is an extensively used elastomeric material for soft lithography. On the other hand, other siloxane formed polymers can be used in producing molds. PDMS has some advantageous properties that make it most preferred elastomer. It has 1 MPa stiffness value and stiffness value can be varied by altering

precursor polymer and curing agent. Elasticity of PDMS prevents cracking while removing from surface after casting. Furthermore, it provides optical transparency that is important for some applications. Surface properties and chemical structure can be modified by oxidization if it is needed. Additionally, biocompatibility of PDMS is great and it is commercially available [19].

Soft lithography and PDMS is preferred as a result of their unique properties for biomimetic studies. In literature, different natural materials and tissues are copied by using PDMS to get their extraordinary properties. For instance, lotus leaf has a self-cleaning surface, which is extremely hydrophobic. Micro and nano structures of lotus leaf was mimicked with the help of soft lithography. PDMS mold was used for replication of self-cleaning surface [20]. In addition to this, mosquito eyes' exceptional structure demonstrates anti-fogging property. In humidity, superhydrophobic micro and nanostructures helps to get clear vision. Similar structures of eyes were created by using soft lithography and PDMS [21]. On the other hand, eyes of moth were copied with using PDMS and soft lithography to mimic anti-reflective optical properties. The size of nanostructures was 200 nm high and 100-120 nm wide [22]. In conclusion, it can be said that using soft lithography provides ability to copy natural micro and nanostructures. Also, using this technique is easy and cost-efficient.

2.9 Material Choice

Scaffold design and material science approach plays a vital role to construct efficient extracellular matrix analog. For this aim, researchers have advanced some approaches to find the best. In nature, different types of biomaterials such as biodegradable and non-degradable are found but their properties are needed to be developed. Although first applications of bone tissue regeneration had been done by non-degradable biomaterials such as metals, biodegradable materials such as polymers are chosen in recent studies. Most common and popular biomaterial types to construct a well-organized scaffold are osteoinductive materials, hybrid material and hydrogels.

2.9.1 Osteoconductivity

In biomaterials science, osteoconduction defines bone formation between implanted materials and natural tissue. Osteoconductive biomaterials, such as bioglass, calcium phosphates and porous structured biopolymers have been extensively used to get better bone regeneration capacity. Furthermore, addition or surface modification of such biomaterials enables to guide bone formation during regeneration process. Calcium phosphates based materials are commonly chosen as osteoconductive biomaterials since bone tissue is mostly constructed by calcium phosphate based HA. It provides a suitable environment to form natural apatite molecules that are synthesized by osteogenic cells. In literature, some studies were conducted to demonstrate importance of osteogenic cell induction and proved that the cells become more effective to form natural apatite surface when they are stimulated by osteoconductive biomaterials [23].

2.9.2 Osteoinductivity

Osteoinductive biomaterials are capable of inducing bone formation and their usage in bone tissue engineering is very favored and efficient. Numerous kinds of osteoinductive biomaterials are available. Phosphate contained ceramics are osteoinductive materials and their composites are eligible to induce osteogenic molecular mechanisms. HA is a osteoinductive material, which is the most abundant in the natural bone tissue. When osteoinductive agents are formed on the surface of biomaterial, direct interaction of surrounding cells and the agents are observed. As a result of direct interaction, cell differentiation, proliferation and viability increases. In other way, osteoinductive components can be released within time with degradation of scaffold and cell behavior can be controlled [24].

To get well-engineered scaffolds, biomaterial surface can be modified or hybrid materials can be formed. When tissue engineering is considered, a scaffold must have appropriate physical, chemical and biological properties. In case of surface modification is insufficient, blend of different materials might be useful to produce affective

scaffold. There are many studies, which indicate that polymer-polymer or polymer-ceramic blends offer great effectiveness to enhance functionality of bone tissue scaffolds. Composition of HA and polymers are very popular in the literature and it was demonstrated that addition of HA, which demonstrates osteoinductivity bone formation. Furthermore, mechanical properties of polymers can be adjusted with regulating HA concentration [24].

On the other hand, hydrogels are hydrophilic polymer structure, which is able to absorb water and commonly used in bone tissue engineering because of their distinctive physical characteristics. After implantation, minimal tissue damage and immunological responses are created since their perfect biocompatibility. Hydrogel is a 3D network, which is modeled by polymer chains and cross-linkers. Solvent absorption ability is very significant for cell adherence, proliferation and differentiation. Alteration in cross-linker and polymer ratio gives chance to do arrangement in mechanical properties. In case of bone tissue engineering, mechanical properties can be tuned by adding ceramic materials such HA, demineralized form of bone matrix and calcium carbonate. On the other hand, supplementation of calcium and phosphate including materials serves to form osteoinductive environment [25].

2.9.3 Biodegradable Polymers in Bone Tissue Engineering

Polymer based biodegradable materials are preferred using in bone tissue engineering and the reason is that their mechanical, physical and chemical properties are controllable. Furthermore, high ability to mimic ECM environment is possible with biopolymers. On the other hand, their residues after degradation can be resorbed by living organism and degradation rate can be controlled by altering chemical properties. Excellent properties and being controllable makes them extraordinary candidates for bone tissue engineering [26].

Biodegradable polymers can be divided into two main groups, which are synthetic and natural. Most popular synthetic biopolymers in bone tissue engineering are

poly(glycolic acid), poly(lactic acid), poly(p-dioxanone) and their copolymers. On the other hand, collagen, gelatin, albumin and polysaccharide structured chitin, chitosan, alginate, cellulos and hyaluronate are natural biodegradable polymer and used in bone tissue engineering applications. Natural biodegradable polymers are preferred in huge amount of study since they are able to trigger cell attachment and growth and also contain organized structures which mimic ECM [26].

Various types of polymer degradation, namely thermal, mechanical, chemical or optical are possible. Polymer degradation occurs step by step and firstly, polymer chains degrade to oligomers and then oligomers are degraded to monomers. Degradation time takes more time if polymer contains covalent bonds in its chemical structure. In addition, molecular weight changes lead to differences in degradation rate. The process of degradation can be categorized into two groups that are surface and bulk erosion. Surface related type occurs as a result of hydrophobicity of biopolymer and results defects on the surface. On the other hand, bulk erosion is observed when water penetration is possible. In this erosion type, backbone of biopolymer, which may contain hydrolysable bonds is destroyed with interaction of water molecules [27].

2.9.4 Chitosan

Chitosan (CH) is a polysaccharide based biopolymer and formed with deacetylation of chitin, which is abundantly available in nature. CH structure is formed with repetition of N-acetyl-D-glucosamine and D-glucosamine groups. These groups are called as glycosaminoglycan and commonly found in extracellular matrix (ECM) . Figure 2.3 shows chemical structures chitosan [28].

Deacetylation degree (DD) is important factor, which alters properties of CH. It is calculated by the ratio of D-glucosamine to total D-glucosamine and N-acetyl D-glucosamine amount. Deacetylation degree should be 60% to gather CH from chitin at least. Rich amount of chitin is accessible in nature and the main chitin source is crustaceans. Molecular weight of CH can be between 300 and 1000 kDA and it

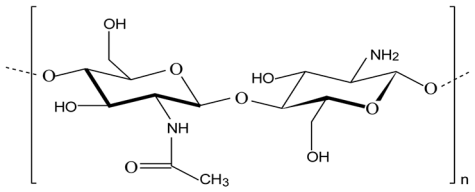

Figure 2.3 Chemical structure chitosan [28].

can also be altered by chemical processes. CH is a biodegradable polymer, which do not create any toxic residues during degradation. Degradation profile is depended on molecular weight and deacetylation degree. Duration of degradation can be controlled by changing these parameters. Since it is obtained from natural resources, it may contain some organic or inorganic contaminants that leads change in its physical and chemical properties. Gradients of CH should be evaluated by physical and chemical characterization techniques before applications [7].

CH has amino groups in its structure and these groups are effective to give various properties. D-glucosamine is able to be protonated and dissolved in diluted acidic solutions with the help of protonation process. Additionally, amino groups provide capability of binding different molecules such as lipids, proteins and anionic ions. As a result, modification of CH biopolymer is possible and amino groups can create covalent bonding. Unique structure of CH is positively charged, which can be used for modification [29].

2.9.5 Chitosan in Bone Tissue Engineering

In bone tissue engineering, CH is a promising material, which comprises excellent biocompatibility, osteoconductivity and induction of osteoblast cell proliferation. Furthermore, it is a biodegradable polymer, which offers prevention of secondary surgery after regeneration. Main drawback of CH is having low osteoinductivity capacity, which

is vital for bone formation [7].

Several applications of CH in tissue engineering has been applied. CH scaffolds can be fabricated in the form of sponges, films and fibrous. Composite scaffolds of CH have been commonly preferred in bone tissue engineering. Blending of different materials into CH solution creates opportunity to enhance drawbacks of it and regulate cell behavior, as well. For instance, HA and CH composite was prepared to mimic bone ECM by Hoctor et al. In this study, it was demonstrated that HA and CH together has better properties for bone tissue engineering [30]. Furthermore, Misra et al. proved that combination of two materials results in enhancement of mechanical, chemical and biological properties of CH. It was suggested that HA addition is promising for mimicking bone tissue [31]. On the other hand, cytotoxicity of HA and CH was tested by Ge et al. After conduction of in vivo degradation test, there was no observable toxicity and it was concluded that these two materials can be used for in vivo applications [32].

2.9.6 Hydroxyapatite

Inorganic compound of bone tissue is mostly formed by HA. It contains calcium and phosphate groups in its structure and general formula of HA is $Ca_{10}(OH)_2(PO_4)_6$. Being most abundant molecule in natural bone tissue makes it extensively used in bone regeneration and tissue engineering. It is used as coating material or fillers, which enables bone repair [33].

HA has several advantageous properties, namely biocompatibility, long degradation duration, excellent osteoconductivity. HA can be produced in nano-size that provides different properties to material. Nano-sized HA is more useful load-bearing applications since it's mechanical strength is enhanced with nanostructure. In addition, nanostructures provide more surface area, which increases fracture toughness [33]. The chemical structure of HA can be seen in Figure 2.4 [34].

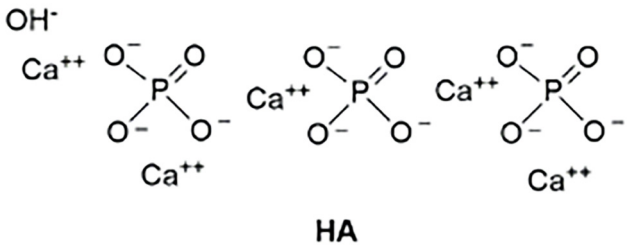

Figure 2.4 Chemical structure of HA [34].

2.9.7 Hydroxyapatite in Bone Tissue Engineering

HA can be blended with biopolymers or surface modification can be conducted for bone tissue engineering applications. Surface modification is beneficial for altering chemical properties of scaffolds. Interaction between designed scaffolds and tissue is among the surface of material and ECM molecules directly attach to scaffold surface. Because of this, surface can be altered with desired properties to create similar environment of ECM. Chemical modification of surface is a promising way to enhance cell adhesion and migration. In bone tissue engineering, nanoparticles of HA are extensively used for surface modification. Bone surface contains great amount of HA nanoparticles and surface modification with HA is important to mimic natural tissue. It was observed that rough surface of HA leads to increase expression of osteoblastic markers and genes. HA increases osteoblastic cell attachment on scaffolds and provides osteoconductivity [8].

In addition, HA surface modification is able to activate mineralization process. High surface area leads to increase of osteoblast cell functions. Nanosized molecule interaction triggers several cellular mechanisms that are vital. When these factors are considered, surface modification helps to fabricate more efficient bone tissue scaffolds [35]. HA influence on CH scaffolds was investigated by Zhang et al. Researchers observed that nano-HA triggers more apatite formation, which is very significant to mimic natural mineralization process when it is compared with pure CH scaffold. Proliferation of cells were more efficient when scaffold surface was coated with nano-HA and alkaline

phosphatase activity, which demonstrated differentiation of cells increased. Lastly, it was concluded that HA addition is a useful method to trigger and enhance bioactivity [36].

2.9.8 Graphene Oxide

Graphene is a carbon based and two dimensional material, which is formed by flakes. It demonstrates exceptional properties and is used in different biomedical applications such as imaging, drug delivery and tissue engineering. Although it is a very popular material, its properties have not been well-defined yet. Extraordinary structure of graphene enables to get outstanding properties and nanostructure provides capability to create better interaction with cells [9].

In addition to graphene, oxidized forms of graphene have synthesized. Graphene oxide (GO) is made of graphene sheet and contains carboxylic acid, epoxy and hydroxyl residues. Monolayer or multilayer forms of GO can be formed. GO is extensively used for composite fabrication in tissue engineering. Functional groups of GO make possible to covalent or non-covalent interactions with other functional groups [15]. In literature, various polymers namely polyethylene glycol (PEG), poly(vinylalcohol) (PVA) and CH has been used with GO that provides better mechanical and chemical properties to these biomaterials. Covalent interaction between CH and GO is done via amide groups of CH and carboxylate group of GO [9].Figure 2.5 shows chemical structure of GO [37].

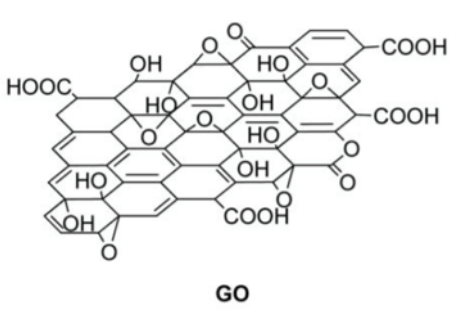

Figure 2.5 Chemical structure of GO [37].

2.9.9 Graphene Oxide in Bone Tissue Engineering

GO influence on mesenchymal stem cells and osteoblasts have attracted researchers since it provides excellent properties that are promising for bone tissue engineering. Adhesion, proliferation and differentiation of cells have been investigated with different researchers and studies. Kim et al. worked on cell adhesion and proved that adhesion of adipose-derived stem cells increased when they interact with GO. In addition, it was found that pre-osteoblast and osteoblast demonstrated better adhesion on CH/GO composite when compared with pure CH scaffolds. On the other hand, proliferation phenomena and GO effect has been investigated in literature. It was observed that GO addition or modification on biopolymers helped to increase proliferation of pre-osteoblasts and osteoblasts [38]. In bone tissue engineering, human mesenchymal stem cells are differentiated to produce osteoblasts. Influence on differentiation was evaluated by Ozyilmaz et al. They demonstrated that GO results a speed differentiation of human mesenchymal stem cells [39]. In other study, chemical vapor deposition of GO was used to coat SiO2 surface. When coated and non-coated surface results compared, higher proliferation of human osteoblasts was observed [40].

GO addition in CH biopolymer has been remarkably studied in bone tissue engineering since each of two materials demonstrates tailor-made properties for bone tissue applications. For this aim, in vitro cytocompatibility of CH/GO scaffolds was tested by Hermenean et al. Murine pre-osteoblast cell line was chosen to conduct cytotoxicity test. Researchers concluded that GO addition in CH offers great potential for bone tissue engineering since it triggers cell growth and proliferation. In addition, composite scaffolds demonstrated great biocompatibility and release of cytotoxic agents was not observed during the study. When biocompatibility, cell induction and enrichment of mechanical properties are considered, it can be concluded that GO is a promising candidate for bone tissue engineering and offers great potential [41].

3. MATERIALS and METHODS

3.1 Bovine Femur Cleaning Process

Bone surface was mimicked by using bovine femur and it was gathered from butcher. Before mimicking process, small pieces of bone were obtained via cutting with the help of a saw. Bone must be cleaned before mimicking process since some chemical might contaminate bone or it may contain some biological agents namely, viruses and bacteria. Cleaning procedure contains different steps and Figure 3.1 demonstrates required bone surface cleaning procedure before mimicking process [42].

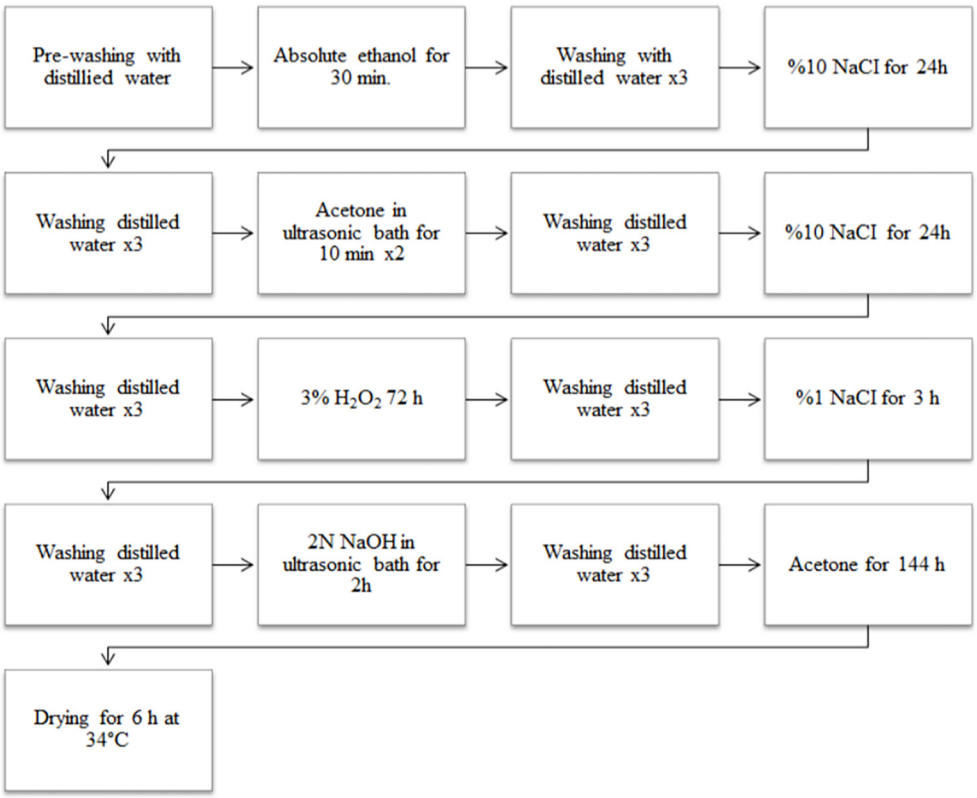

Figure 3.1 Bone surface cleaning diagram [42].

3.2 Experimental Groups

Eight different experimental groups were used in this thesis to understand effect of bone surface topography and chemical composition on human osteoblast cells. All experimental groups were listed in Table 3.1.

Table 3.1
Experimental groups.

Experimental Groups
Plain CH
Plain CH/GO
Bone Surface Mimicked CH
Bone Surface Mimicked CH/GO
HA Modified Plain CH
HA Modified Plain CH/GO
HA Modified Bone Surface Mimicked CH
HA Modified Bone Surface Mimicked CH/GO

3.3 Bone Surface Mimicking

Bone surface topography and microstructures were mimicked by polydimethylsiloxane (PDMS) and soft lithography technique. PDMS is composed of silicone elastomer and curing agent and for getting ideal mimicking, the ratio of silicone elastomer and curing agent was chosen as 10:1, respectively. Silicone elastomer and curing agent was mixed as far as homogenous blend was obtained. Mixing process causes bubbles in the structure of PDMS solution and effects mimicking ability. Because of this reason, degasing process was applied via desiccator to get rid of bubbles.

In the next step, homogenous PDMS solution was casted on cleaned bone surfaces and baked for 4 hours at 70°C. When curing of PDMS was completed, bone was gently separated from PDMS. After all these procedures, PDMS had copied bone surface structures on it's surface and mimicked PDMS was used as a mold to fabricate bone surface mimicked biopolymer membranes [42].

3.4 CH Purification

During CH membrane fabrication, low molecular weight CH powder was used and purchased commercially from Sigma-Aldrich. Commercial CH powder included some contaminant gradients, which might influence on mimicking ability. As a result of this problem, purification procedure was conducted before mimicking process.

Firstly, CH is able to be dissolved in diluted acetic acid and its solution was prepared by using diluted acetic acid. 10g CH powder was dissolved in 1 liter of 1%v/v acetic acid. The solution was mixed with mechanical stirrer overnight to obtain homogenous solution. Homogenized solution was filtered to get rid of some of the impurities. 20-25 μm pore sized commercial filter paper was used.Gelation of CH is related to pH value, so that pH adjustment process was done with supplementation of NaOH. Before pH adjustment, 1M NaOH solution was prepared via mixing 40g NaOH and 1 liter distilled water. NaOH solution was slightly added into the CH solution and pH value was controlled with pH paper. CH solution was mechanically mixed during addition of NaOH. The pH value of CH solution was set between 10-12 .

After this step, solution was poured in falcon tubes and centrifuged at 1000 rpm for 10 minutes and supernatant was removed. Rest material was washed with deionized water and centrifuged, again. Washing with deionized water and centrifuge step was repeated for 3 times to remove residuals impurities. At last, supernatant was again decantated from the tubes and purified CH was collected. Purified CH was stored in a sterile cup at -20°C for 24 hours. After 24 hours, it was heated and water inside of it's structure was removed. Lastly, remaining pure CH was dried at 40°C for 48 hours

on hotplate and became ready to use [43].

3.5 Fabrication of CH Membrane

Bone surface mimicked and plain CH membranes were fabricated from purified CH. Purified CH was dissolved in diluted 3%v/v acetic acid and deionized water. 66 ml of 3%v/v solvent was added on 2g of purified CH and two of them mixed, mechanically. To overcome viscosity and dissolution problem, whole volume of the solution was fulfilled to 80 ml with deionized water. The solution mixed for 5 hours to obtain homogeneity. Bone surface mimicked PDMS was used as a mold and CH solution was casted on PDMS surface to fabricate mimicked membranes. On the other hand, plain CH membranes, which was used in cell studies were casted in 48 well-plates. 500 μl of the solution was poured in each well. Casted CH solutions were dried at 35°C for 48 hours. After this step, 1M NaOH was treated with the membranes for 5 hours to inactive acetic acid residues. Lastly, the membranes were washed with deionized water to remove remaining NaOH residues and then they were dried at room temperature for 24 hours [44].

3.6 Fabrication of CH/GO Nanocomposite Membrane

GO aqueous solution (2mg/ml) was purchased from Sigma Aldrich. First of all, purified CH was dissolved in diluted 3%v/v acetic acid and water. 66 ml of 3%v/v added on 2g of purified CH and two of them mixed, mechanically for 5 hours. Total volume of CH solution was diluted to 75 ml with the help of deionized water to overcome dissolution problem. In addition, 2 ml of GO solution was taken and diluted to 5 ml with deionized water. GO flakes were homogenized via digital homogenizator for 30 minutes. After that, CH solution and GO solution were mixed and homogenized for 1 hour, again. When this step was completed, mixture of CH and GO was mechanically mixed for 3 hours to get homogeneous dispersion.

Bone surface mimicked PDMS was used as a mold and CH/GO solution was casted on PDMS surface. Furthermore, plain CH/GO nanocomposite membranes were casted in 48 well-plates for cell studies. 500 μl of the solution was poured in each well and dried at 35°C for 48 hours. After drying, 1M NaOH was treated with the membranes for 5 hours to inactive acetic acid residues. Consequently, the scaffolds were washed with deionized water to remove remaining NaOH residues and then they were dried at room temperature for 24 hours [45].

3.7 HA Modification of Membranes

CH and CH/GO nanocomposite membrane surfaces were modified with HA to increase osteoconductivity and osteoinductivity. 1%w/v HA solution was prepared with using 100% ethanol as a solvent. Before dissolving HA, ethanol was waited at 4°C since cold ethanol is more efficient to dissolve. HA solution was stirred at least for 1 hour to make a homogeneous solution.

UV/Ozone treatment was conducted for modifying fabricated membranes. Various time exposures such as 1,2 and 5 minutes were applied. After UV/Ozone treatment, homogeneous HA solution was added on the membranes and waited for 24 hours. During waiting process, stirrer was used not to loose homogeneity of HA solution. The success of modification was assessed by chemical characterization techniques such as FT-IR, XPS, XRD and Raman spectroscopy.

3.8 Characterization Techniques

Modified and non-modified CH and CH/GO nanocomposite membranes were characterized by various techniques such as mechanical, morphological and chemical.

3.8.1 Swelling Capacity Test

Water intake of plain and bone surface mimicked membranes were analyzed by swelling test. Before the test, membranes were dried at 40°C overnight to remove water inside. The dried membranes weights were measured and recorded. After that, membranes were placed in PBS, which mimics in vivo environment. Weights of the membranes were measured again at specific time points, namely 5,10,30 minutes,1,2,3,4 and 24 hours. Swelling ratio was calculated with the help of the difference between initial and the last weight [46].

3.8.2 Water Contact Angle Measurements

Wettability phenomena was assessed with contact angle test. For contact angle test, a drop of PBS was used. Sample size was chosen as four and measurement was conducted during 10 minutes to observe time relationship. The polymeric membranes were stabilized on microscope slide with the help of sticky tape. Middle side of the sticky tape where the PBS droplet falls was removed before this procedure to prevent interaction of tape and droplet.

3.8.3 Confocal Microscopy Analysis

Bone mimicking ability and surface roughness of CH membrane was investigated via confocal microscopy analysis (Zeiss LSM 800 System). Height map of plain and bone surface mimicked CH membranes were analyzed and also their images were captured.

3.8.4 Scanning Electron Microscopy(SEM) Imaging

Surface of plain and bone mimicked CH were investigated by SEM imaging to confirm bone surface structures mimicking ability of CH. In addition, CH/GO nanocomposite membranes were imaged to observe GO on the surface.

On the other hand, SEM imaging was conducted after UV/Ozone treatment to understand surface deformation is found or not. Before imaging process, membranes were coated with 50 nm thick gold layer and the Philips XL30 ESEM-FEG/EDAX was used at 5.00 kV. Additionally, HA modified surfaces were imaged to observed nanoparticles with SEM/EDS at 15.0 kV and their Ca/P ratio was calculated.

3.8.5 FT-IR Analysis

Chemical composition of each membrane was investigated by using FT-IR. Data was recorded over the range of 4000 to 400 cm^{-1}. Efficient UV/Ozone time exposure for HA modification was decided by considering FT-IR peaks. The analysis was conducted at Hacettepe University, Department of Chemistry.

3.8.6 Raman Spectroscopy Analysis

Chemical composition of membranes and HA modifications were analyzed by using Renishaw inVia Qontor Raman Spectroscopy. Analysis was conducted with 785 nm laser wavelength.

3.8.7 XPS Analysis

Atomic composition of membranes was evaluated by using Thermo Scientific K-Alpha XPS Spectrometer. Survey scan and binding energy (eV) values between 0 and

1000 was obtained. Atomic percentages of chemical components were calculated. The analysis was performed by using Thermo Scientific Spectrometer at Bogazici University.

3.8.8 Methylene Blue Staining

Methylene Blue staining method was applied to evaluate activation of carboxyl groups of CH and ability of binding to cationic molecules. 0.1% aqueous methylene blue solution was prepared by mixing at room temperature. Various time exposures of UV/Ozone such as 1,2 and 5 minutes were applied to membranes and methylene blue solution applied for 1 hour to membranes [47].

3.8.9 XRD Analysis

XRD analysis was performed by using CuKa light source with 1.54 A° wavelength.The data range was selected between 4-80° with the step size of 0.050° [48]. The analysis was performed by using PANalytical XPert system at Yildiz Technical University.

3.9 Cell Culture Study

hFOB 1.19 human fetal osteoblasts were purchased from ATCC and used in the experiments. The cells were cultured in an incubator, which is set to 5% CO_2 and 35.5°C. DMEM/F-12 Medium with 10% fetal bovine serum (FBS) and 1% penicillin-streptomycin antibiotic was used during cell culturing[49]. The medium was changed in two days period and washing with PBS was conducted before medium changing. Before cell seeding into well plates, cells were detached with trypsin-EDTA solution for 5 minutes at 35.5°C. Detached cells were observed with microscopy and fresh medium was added to inactivation of trypsin. Centrifugation at 1000 rpm with 5 minutes was done to gather cells from suspension and then cells were resuspended with fresh

medium. Cell counting was conducted using hemocytometer and 1x10^4 cells were seeded in 48-well culture plates.

Fabricated membranes were sterilized with 70% ethanol for 2 days and washed with PBS. In addition, the membranes were waited in the medium overnight to get rid of ethanol residues, completely. Lastly, twice washing with PBS was conducted.

3.9.1 MTT Assay

Five samples from each experimental group were placed into 48-well culture plates. Approximately, 1x10^4 cells with 300 μl were seeded into wells. Cell seeded membranes were incubated at 35.5°C. The medium was replaced every two days. 30 μl MTT solution (5mg/ml) was added into the medium and incubated for 3.5 hours at 35.5°C. Then the solution was removed and 150 μl DMSO was added into wells. Optical density was analyzed at 490 nm with the help of microplate reader [50].

3.9.2 SEM Imaging

Morphology of seeded cells were evaluated at day 7 and fixation procedure was conducted before imaging. 2.5% glutaraldehyde solution was added into each well and waited for 1 hour at 4°C. The solution was removed and samples were waited in PBS at 4°C. The stored samples were dehydrated in 50%, 70%, 90% and 100% ethanol for 3 minutes and hexamethyldisilazane (HMDS) for 5 minutes. Lastly, the samples were dried overnight and SEM cellular morphology imaging was done [48].

4. RESULTS

4.1 SEM Images of Mimicked Surfaces

Bone surface structures were copied by using soft lithography technique and polymeric membranes, which have bone micro and nanostructures on their surfaces were fabricated with solvent casting process. SEM imaging was conducted to analyze mimicking ability of CH and CH/GO based polymeric membranes and similar surface structures with natural bone were observed. SEM images of bone and bone surface mimicked membranes' were shown in Figure 4.1.

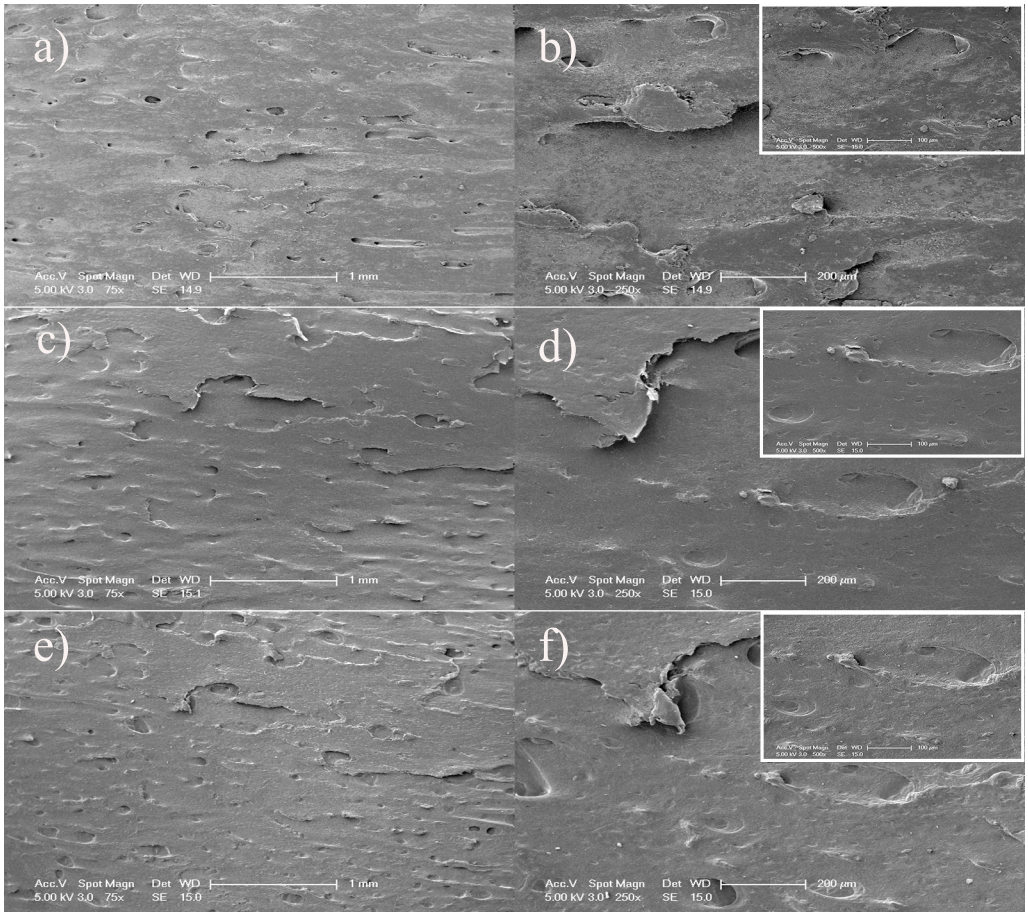

Figure 4.1 Surface of bone, CH and CH/GO membranes were evaluated by SEM imaging. a) Bone surface (75x) b) Bone surface (250x and 500x) c) BSM CH membrane surface (75x) d) BSM CH membrane surface (250x and 500x) e) BSM CH/GO nanocomposite membrane surface (75x) f) BSM CH/GO nanocomposite membrane surface (250x and 500x).

4.2 Confocal Microscopy Analysis

Confocal microscopy analysis was conducted to determine the roughness difference between plain and bone surface mimicked membranes. 3D view and texture images of the scaffolds were obtained. Significant roughness value differences observed with plain and bone mimicked surfaces. Plain CH had the value of 56.992 nm, while BSM CH had 5.245 μm. Height map and texture images of plain and bone surface mimicked surfaces were obtained with confocal microscope and demonstrated in Figure 4.2-4.4.

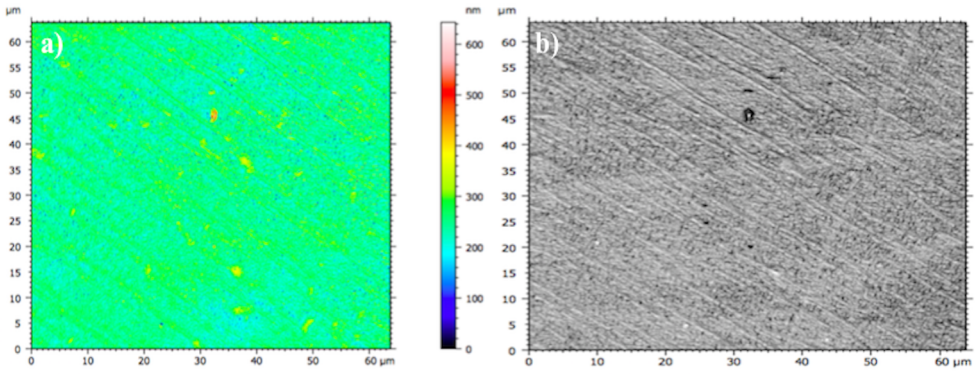

Figure 4.2 a) Height map of plain CH membrane (50x) b) Texture image of plain CH membrane (50x).

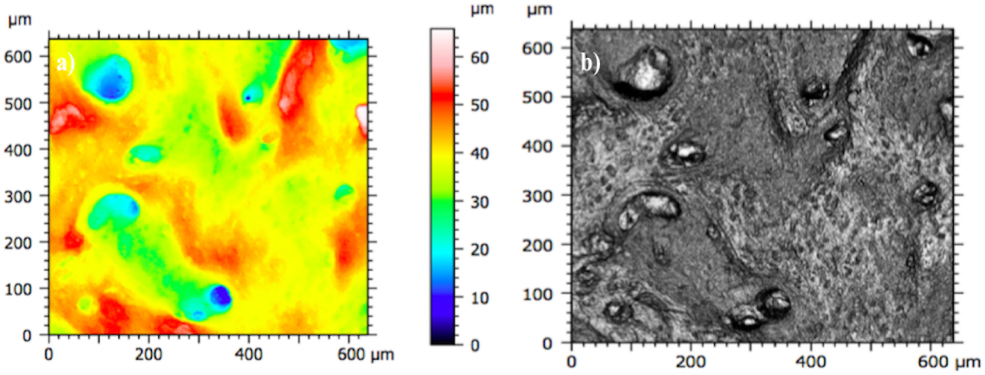

Figure 4.3 a) Height map of bone surface mimicked CH membrane (10x) b) Texture image of bone surface mimicked CH membrane (10x).

The roughness values and profiles of plain CH and bone surface mimicked CH were listed in Table 4.1. Sa and Sq parameters define average roughness values of membranes and Ssk indicates skewness of the membranes. Negative Ssk value defines that surface is dominated by valleys. Sp and Sv terms are used to define maximum

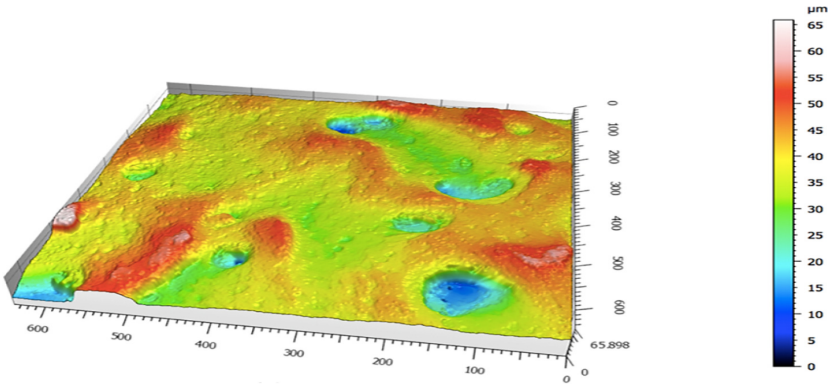

Figure 4.4 3D view of bone surface mimicked CH membrane.

profile peak height and maximum valley depth, respectively. Sz is average of the five highest peaks and deepest valleys [51].

Table 4.1
Roughness values of plain and BSM CH.

Height Parameters	Plain CH	BSM CH
Sa	56.992 nm	5.245 μm
Sq	72.646 nm	7.139 μm
Ssk	0.423 nm	-0.703 μm
Sp	664.445 nm	26.988 μm
Sv	225.870 nm	38.910 μm
Sz	920.314 nm	65.898 μm

4.3 Swelling Test

All swelling experiments were conducted by using phosphate buffer solution(PBS) to mimic in vivo environment in terms of pH and swelling capacity was measured within specific time intervals, which was listed in Table 4.2. The swelling ratio of plain CH membrane increased to 120.53% after 24 hours, while BSM CH membrane had greater increase that was 152.22%. GO addition increased swelling ratio in plain membranes and plain CH/GO nanocomposite membranes had the value of 136.89% after 24 hours.

On the other hand, GO addition to BSM membranes resulted a slight decrease in swelling capacity. BSM CH/GO nanocomposite membranes had 145.27%, which was less than plain CH/GO membranes. The complete swelling ratio of fabricated membranes was given in Table 4.2.

Table 4.2
Swelling ratios of membranes.

	Swelling Ratio (%)			
Time	Plain CH	BSM CH	Plain CH/GO	BSM CH/GO
5min	103.31±3.93	119.54±6.25	115.97±1.06	113.15±9.64
10min	108.93±2.86	137.05±5.32	119.76±1.42	138.83±13.04
30min	110.91±3.24	141.43±2.23	120.05±3.81	141.12±0.83
1h	114.15±3.03	143.74±2.95	122.57±5.76	142.16±0.98
2h	113.68±1.79	145.92±2.02	128.20±3.62	142.08±1.40
3h	114.86±2.50	147.19±2.08	129.33±3.46	142.68±0.49
4h	115.45±3.21	147.31±1.32	129.78±2.02	143.51±0.91
24h	120.53±2.23	152.22±1.98	136.89±2.56	145.27±1.11
Mean	112.72±4.77	141.80±9.4	125.31±6.44	128.60±9.77

To compare differences between all groups, one-way ANOVA and Tukey's HSD test were conducted. Six different comparison groups were gathered and the results were shown in the Table 4.3.

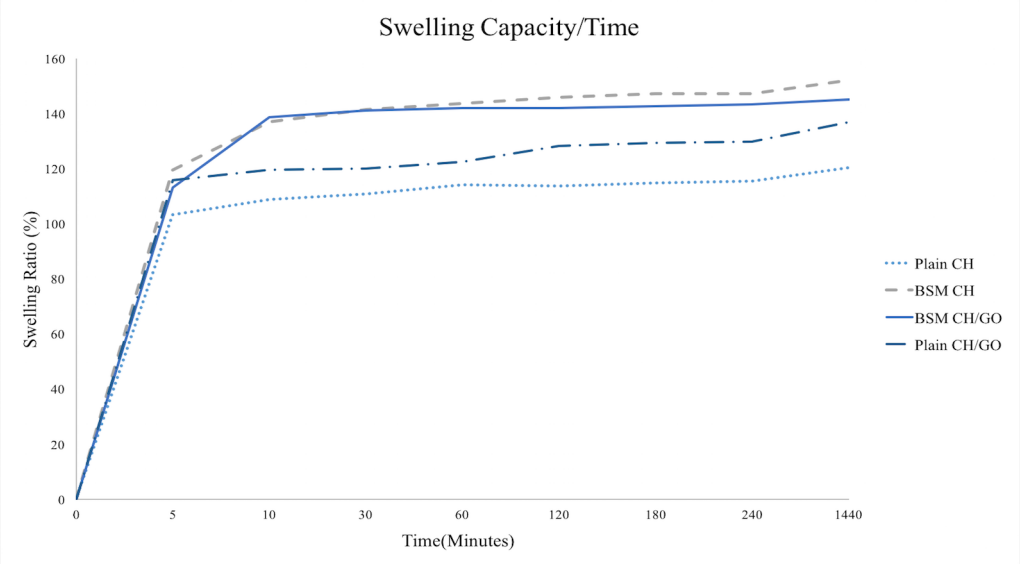

Figure 4.5 Measurement of swelling ratio of plain CH, BSM CH, plain CH/GO and BSM CH/GO membranes with using PBS over 24h.

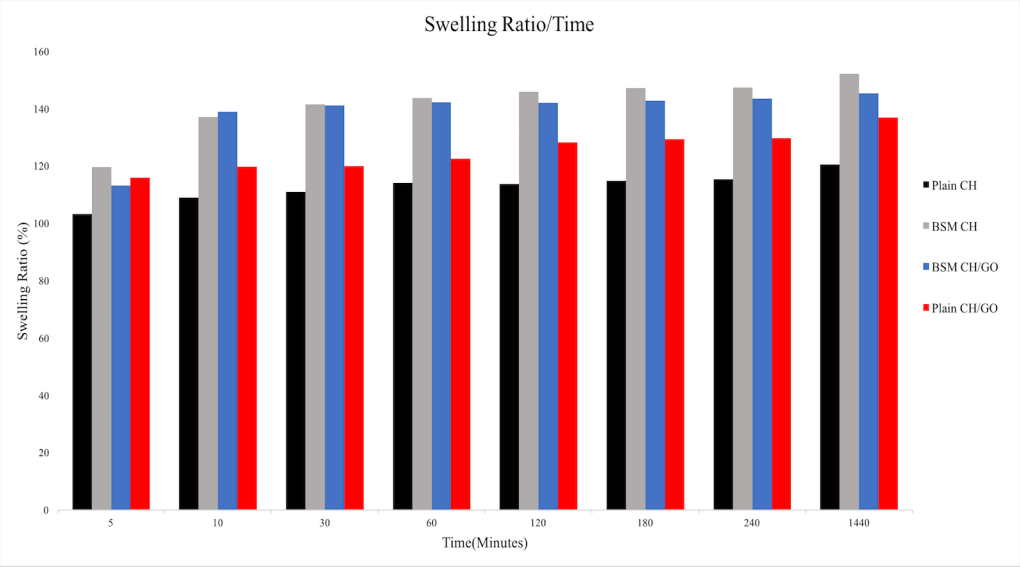

Figure 4.6 Measurement of swelling ratio of plain CH, BSM CH, plain CH/GO and BSM CH/GO membranes with using PBS over 24h.

Table 4.3
Swelling capacity comparison of groups.

Sample Group 1	Sample Group 2	Swelling Capacity	p value
Plain CH	BSM CH	BSM CH>Plain CH	$p<0.01$
Plain CH	BSM CH/GO	BSM CH/GO>Plain CH	$p<0.01$
Plain CH	Plain CH/GO	Plain CH/GO>Plain CH	$p<0.01$
BSM CH	BSM CH/GO	BSM CH>BSM CH/GO	Non-significant
BSM CH	Plain CH/GO	BSM CH>Plain CH/GO	$p<0.01$
BSM CH/GO	Plain CH/GO	BSM CH/GO>Plain CH/GO	$p<0.05$

4.4 Water Contact Angle Measurements

Hydrophilic properties of membrane surfaces were analyzed with water contact angle measurements and PBS solution was used for the test to mimic in vivo pH conditions. The droplet shape of PBS was observed during 10 minutes and images were captured. Plain CH membranes, which had 74.52° contact angle value after 10 minutes demonstrated hydrophilicity. BSM CH membranes had the value of 69.04° and showed more hydrophilicity than plain CH membranes. Plain CH/GO was considered as the most hydrophilic membrane with showing 63.95°. In contrast, BSM CH/GO membranes had 83.36° and were the least hydrophilic group. Water contact angle values of plain and BSM membranes were listed in Table 4.4.

Table 4.4
Water contact angle values of membranes by using PBS over 10 minutes.

	Water Contact Angle(°)			
Time(Min)	Plain CH	BSM CH	Plain CH/GO	BSM CH/GO
1	88.99±3.53	84.13±3.76	85.87±2.71	98.08±1.57
2	87.09±2.43	79.68±3.62	82.50±2.29	96.61±1.36
3	85.43±3.24	76.87±3.70	79.43±2.14	95.02±1.50
4	83.11±4.96	75.31±3.80	76.13±2.45	93.47±1.18
5	82.25±4.04	74.47±3.47	73.49±3.22	91.64±0.98
6	81.36±3.70	74.15±3.03	72.67±1.48	89.90±0.89
7	80.17±3.49	73.63±3.25	70.76±1.57	88.02±1.17
8	78.56±3.07	72.87±2.66	68.27±1.58	86.38±1.52
9	77.22±2.87	71.48±3.11	65.93±1.53	84.86±1.83
10	74.52±1.96	69.04±3.03	63.95±1.61	83.36±2.14

Graph of water contact angle within 10 minutes and comparison of each group were listed in Figure 4.7 and Table 4.5, respectively. Statistical analysis was conducted considering final contact angle values via using one-way ANOVA and Tukey's HSD test.

Change of droplet was observed when all groups were compared. Bone surface mimicking provided decrease in contact angle. In addition, GO addition was beneficial to obtain lower contact angle values and wetting property. On the other hand, bone surface mimicked and GO added membranes demonstrated highest contact angle value that means hydrophobicity is dominant.

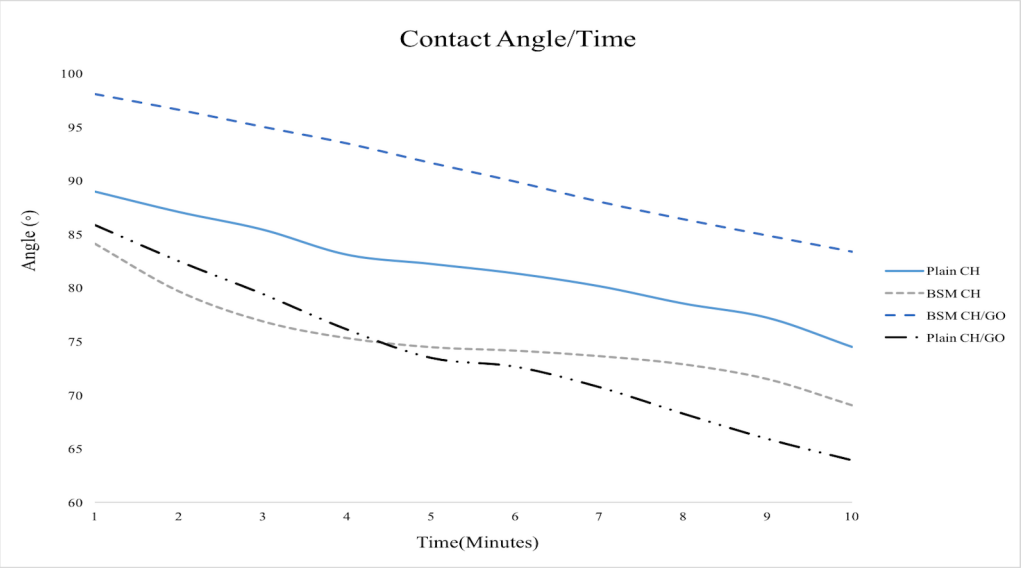

Figure 4.7 Measurement of water contact angle of plain CH, BSM CH, plain CH/GO and BSM CH/GO membranes with using PBS over 10 minutes.

Table 4.5
Water contact angle comparision and statistical analyzes of membranes.

Sample Group 1	Sample Group 2	Water Contact Angle	p value
Plain CH	BSM CH	Plain CH>BSM CH	$p<0.05$
Plain CH	Plain CH/GO	Plain CH>Plain CH/GO	$p<0.01$
Plain CH	BSM CH/GO	BSM CH/GO>Plain CH	$p<0.01$
BSM CH	Plain CH/GO	BSM CH>Plain CH/GO	Non-significant
BSM CH	BSM CH/GO	BSM CH/GO>BSM CH	$p<0.01$
Plain CH/GO	BSM CH/GO	BSM CH/GO>Plain CH/GO	$p<0.01$

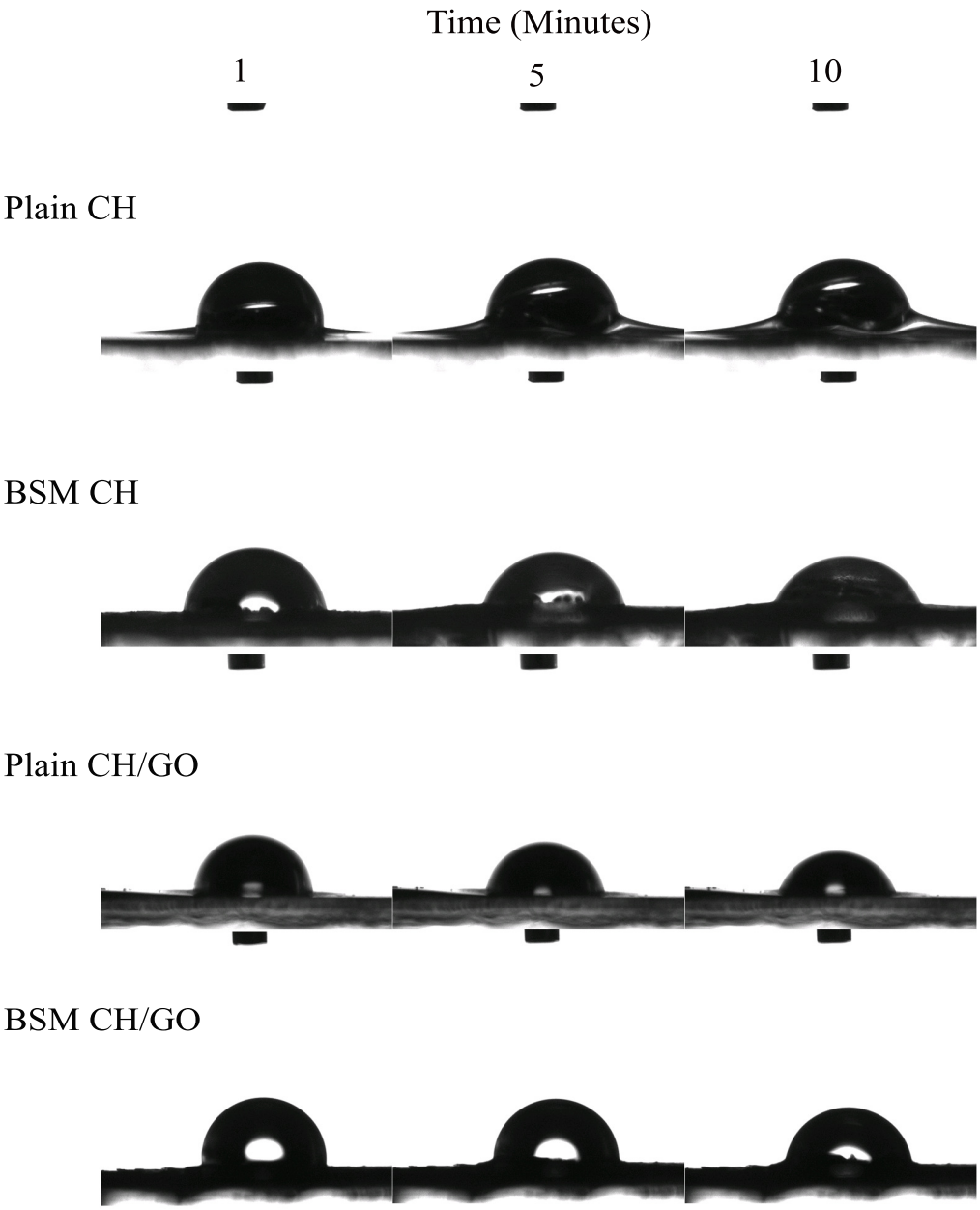

Figure 4.8 PBS droplet formation on fabricated membranes at 1, 5 and 10 minutes.

4.5 Methylene Blue Staining

Methylene Blue staining method was applied to evaluate activation of carboxyl (-COOH) groups of CH and ability of binding to cationic molecules. For this aim, various time exposures of UV/Ozone were applied to scaffolds. After staining procedure, it was concluded that carboxyl groups of CH indicate activity to bind cationic ions. Color change of membranes were demonstrated in Figure 4.9.

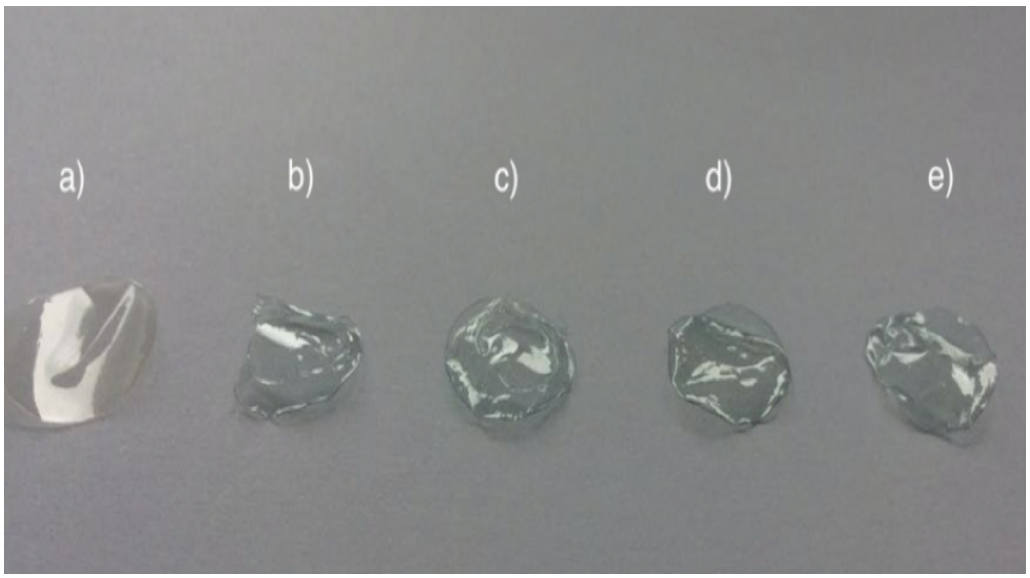

Figure 4.9 Digital photographs of methylene blue staining of UV/Ozone treated CH membranes a) CH membrane without any treatment and staining b) CH membrane without treatment c) 1 minute CH d) 2 minutes e) 5 minutes.

4.6 FT-IR Analysis

HA modification time optimization of CH membranes was decided by evaluation of FT-IR results. 1,2 and 5 minutes UV/Ozone treatment and HA binding capacity was analyzed considering specific peaks, which belongs to HA. Figure 5 demonstrates FT-IR spectra of CH and HA modified CH membranes between 4000 cm^{-1} and 650 cm^{-1} and sharp peak around 1030 cm^{-1} that belongs to HA was observed. On the other hand, spectrum between 650 cm^{-1} and 400 cm^{-1} was demonstrated separately since it includes specific and narrow peaks of HA. In this region, two specific peaks of

PO_4^{-3} group were detected at 603 cm^{-1} and 570 cm^{-1}. 4000 cm^{-1}-650 cm^{-1} and 650 cm^{-1}-400 cm^{-1} regions were demonstrated in Figure 4.10 and 4.11.

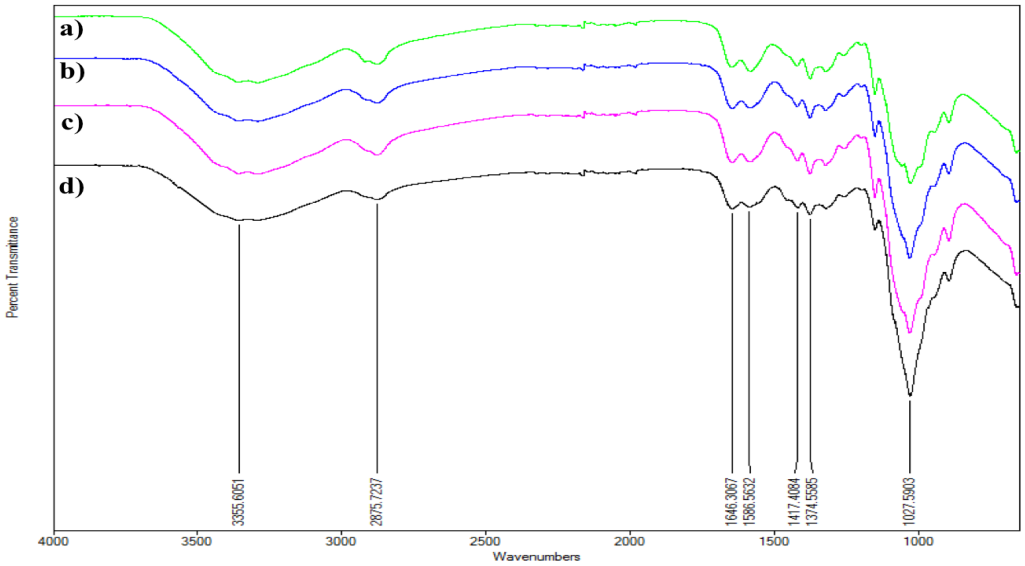

Figure 4.10 FT-IR spectra of a) CH b) CH/HA 1min UV/Ozone treatment c) CH/HA 2 min UV/Ozone treatment d) CH/HA 5 min UV/Ozone treatment 4000 cm^{-1} and 650 cm^{-1}.

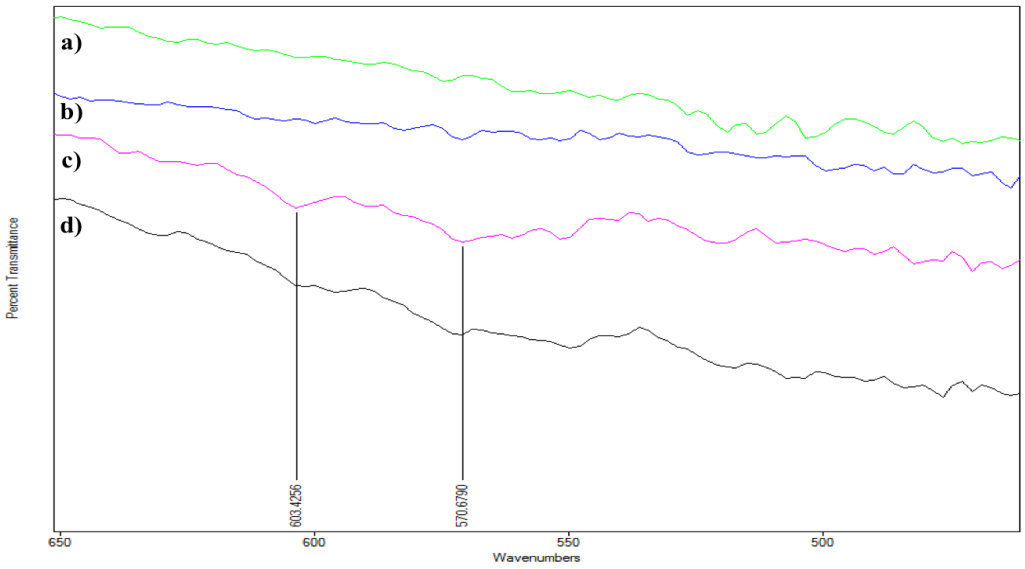

Figure 4.11 FT-IR spectra of a) CH b) CH/HA 1min UV/Ozone treatment c) CH/HA 2 min UV/Ozone treatment d) CH/HA 5 min UV/Ozone treatment 650 cm^{-1} and 400 cm^{-1}.

4.7 SEM Imaging after UV/Ozone Treatment

UV/Ozone treatment was applied before HA modification. SEM imaging analysis was conducted to evaluate surface changes after using high energy treatment. It was observed that there is no changes or degeneration at 1 and 2 minutes UV/Ozone treatment. The surface of membranes demonstrated degenerated areas when they were treated with 5 minutes. As a result of this, UV/Ozone treatment for 5 minutes was eliminated to avoid defects on surface. On the other hand, UV/Ozone treatment was significantly helpful for surface cleaning as expected. Furthermore, GO flakes on surface were observed when nanocomposite membranes were imaged and all images were listed from Figure 4.12 to Figure 4.14.

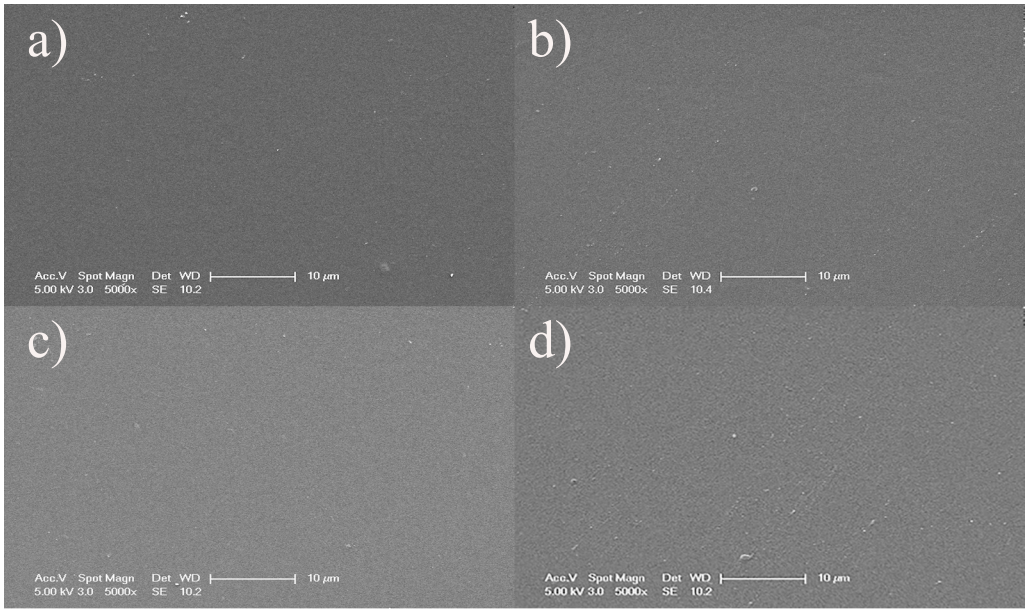

Figure 4.12 SEM images (5000x) of CH membrane were analyzed to observe surface defects after UV/Ozone treatment a) CH membrane without treatment b) 1 minute c) 2 minutes d) 5 minutes.

SEM-EDS analysis was conducted to visualize HA nanoparticles on CH and CH/GO nanocomposite membranes. HA molecules successfully defined on surfaces of two membranes. It was observed that distribution of HA was not uniform.

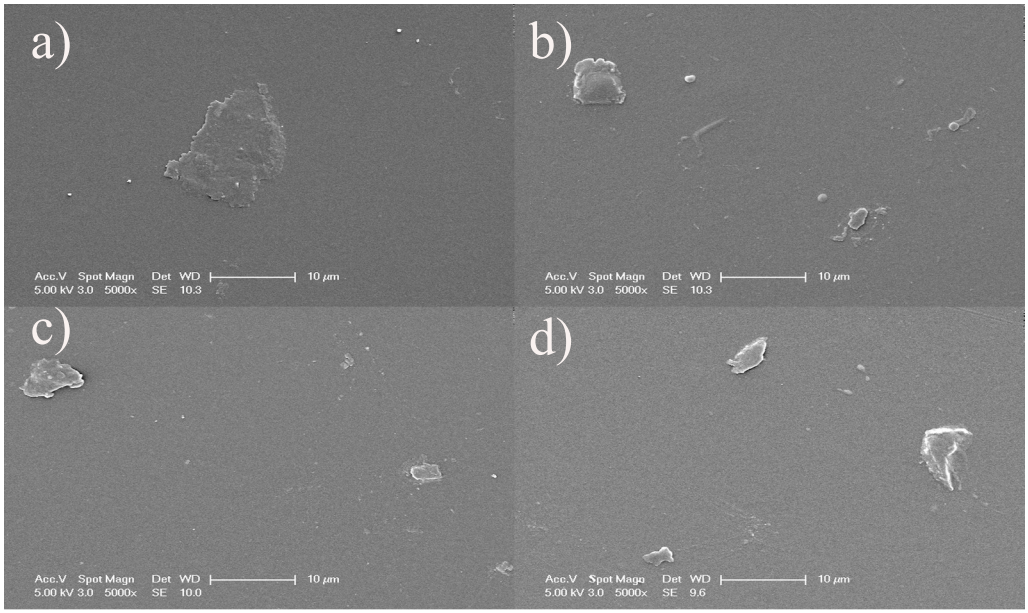

Figure 4.13 SEM images (5000x) of CH/GO nanocomposite membrane were analyzed to observe surface defects after UV/Ozone treatment a) CH/GO nanocomposite membrane without treatment b) 1 minute c) 2 minutes d) 5 minutes .

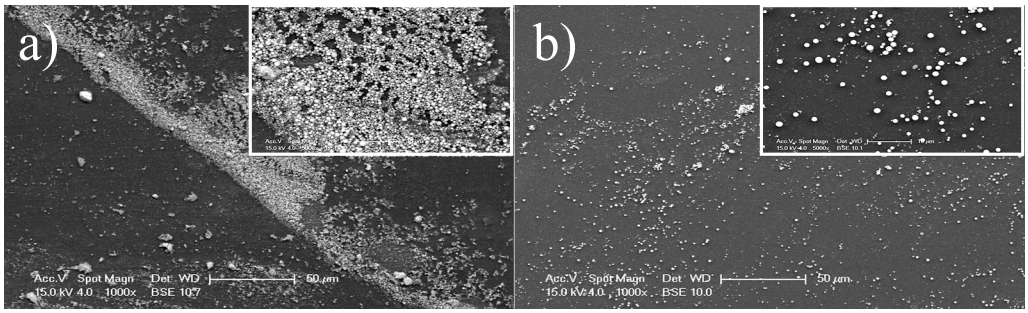

Figure 4.14 HA nanoparticels were indentified on CH and CH/GO membrane surface by SEM. a) HA modified CH membrane (1000x and 5000x) b) HA modified CH/GO membrane (1000x and 5000x).

4.8 XPS Analysis

XPS analysis was conducted to define atomic composition of HA modified CH and CH/GO nanocomposite membranes. Survey scan analysis was done to understand chemical composition. Specific peaks of CH, GO and HA was observed and the data compared with similar works in literature. O1s, N1s and C1s peaks belong to CH chemical structure. In addition, it was indicated that CH and HA interaction results increase of O1s intensity [52]. When O1s intensity was compared with the previous study, which was conducted in our laboratory, increase of intensity was clear [43]. It is known that GO shows O1s and C1s bands [53]. Addition of GO reasoned increase in O1s and C1s intensity. Ca2s, Ca2P, P2s and P2p peaks were observed for each CH and CH/GO membranes and concluded that HA modification was successful.

Survey XPS spectra of HA and modified membranes were shown in Figure 4.15, Figure 4.16 and Figure 4.17.Elemental compositions of membranes can be found in Table 4.6, Table 4.7 and Table 4.8.

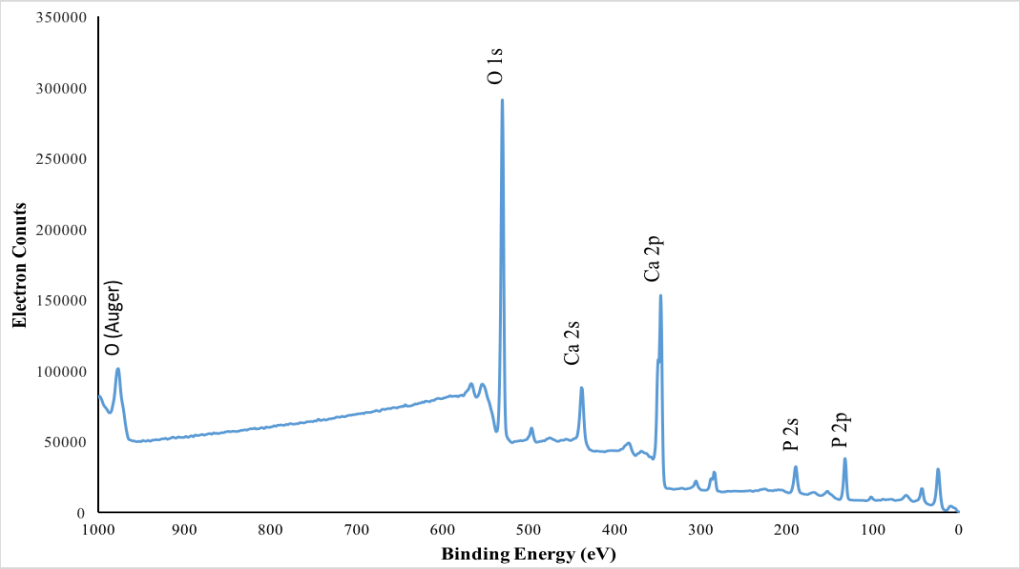

Figure 4.15 Survey scan of HA powder (AlK Alpha Source Gun, Pass Energy 150.0 eV, 300 μm spot size).

Table 4.6
Elemental composition of HA powder.

Elements	Ratio(%)
O1s	31.83
Ca2p	11.95
P2p	7.96
Na1s	1.22
Mg1s	0.5
C1s	7.17
Ca2s	18.66
C1s	7.32
Ca3s	9.7
O2s	3.68

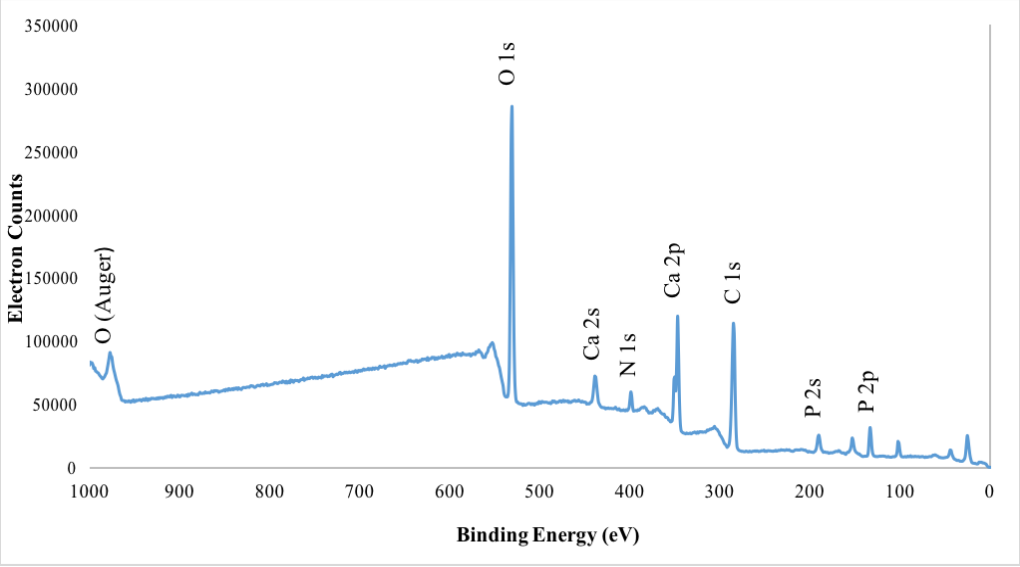

Figure 4.16 Survey scan of HA modified CH membrane (AlK Alpha Source Gun, Pass Energy 150.0 eV, 300 μm spot size).

Table 4.7
Elemental composition of HA modified CH membrane.

Elements	Ratio(%)
O1s	26.92
Ca2p	6.02
P2p	4.66
P2s	4.55
C1s	34.23
Ca2s	9.43
Ca3s	6.25
O2s	2.31
Si2p	3.5

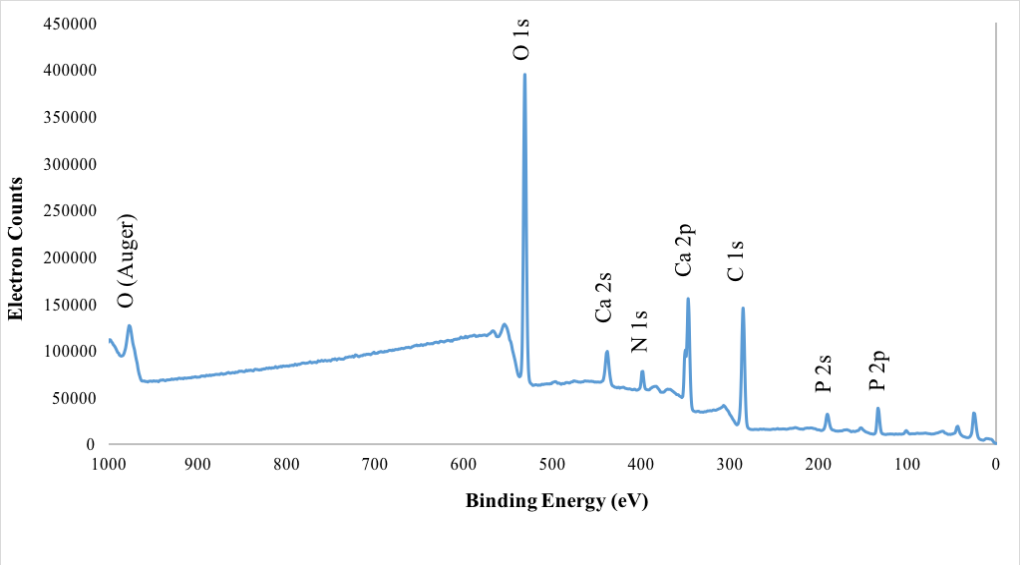

Figure 4.17 Survey Scan of HA modified CH/GO nanocomposite membranes (AlK Alpha Source Gun, Pass Energy 150.0 eV, 300 μm spot size).

Table 4.8
Elemental composition of HA modified CH/GO nanocomposite membranes.

Elements	Ratio(%)
O1s	28.93
C1s	31.86
Ca2p	6.64
P2p	4.78
N1s	2.53
Si2p	0.99
Ca2s	10.71
P2s	4.5
Ca3s	6.64
O2s	2.24

4.9 Raman Spectroscopy

HA modification and chemical composition of membranes were defined by Raman spectroscopy. In addition, GO distribution in membranes were analyzed with the help of D and G bands imaging. Specific HA PO_4^{3-} peaks at around 450, 600 and 960 cm^{-1} was observed on CH membranes. Raman spectra of modified membranes were demonstrated in Figure 4.18 and Figure 4.19.

GO specific D and G bands were observed at 1330 and 1585 cm^{-1}, respectively. In the spectrum of HA modified CH/GO nanocomposite membranes, D and G peak domination was observed and bands shifted to 1318 and 1597 cm^{-1}, respectively. C-H out of deformation of CH structure was observed at 897 cm^{-1}.

GO distribution in membranes were analyzed by D and G peak imaging. It was observed that disturbance of peaks changes in different regions of sample. I_D/I_G value is ranged between 1.364 and 1.616. D and G peak intensity can be seen in Figure 4.20.

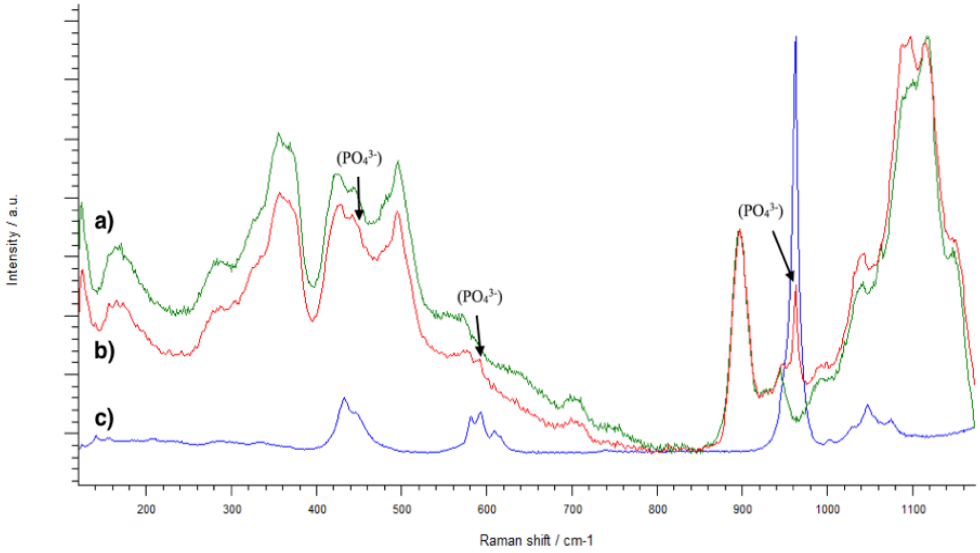

Figure 4.18 Raman spectrum of a) CH membrane b) HA modified CH membrane c) HA powder at 785 nm wavelength.

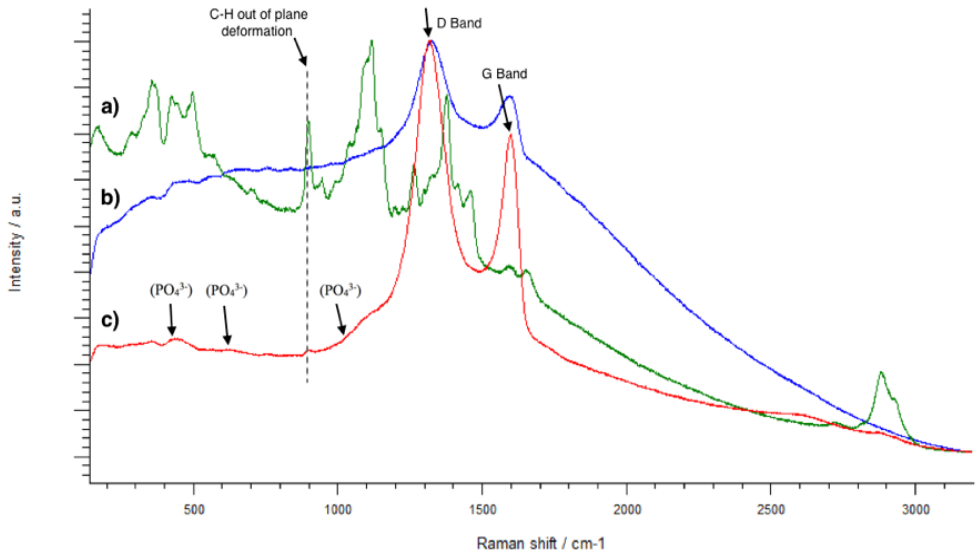

Figure 4.19 Raman spectrum of a) CH membrane b) GO c) HA modified CH/GO nanocomposite membrane 785 nm wavelength.

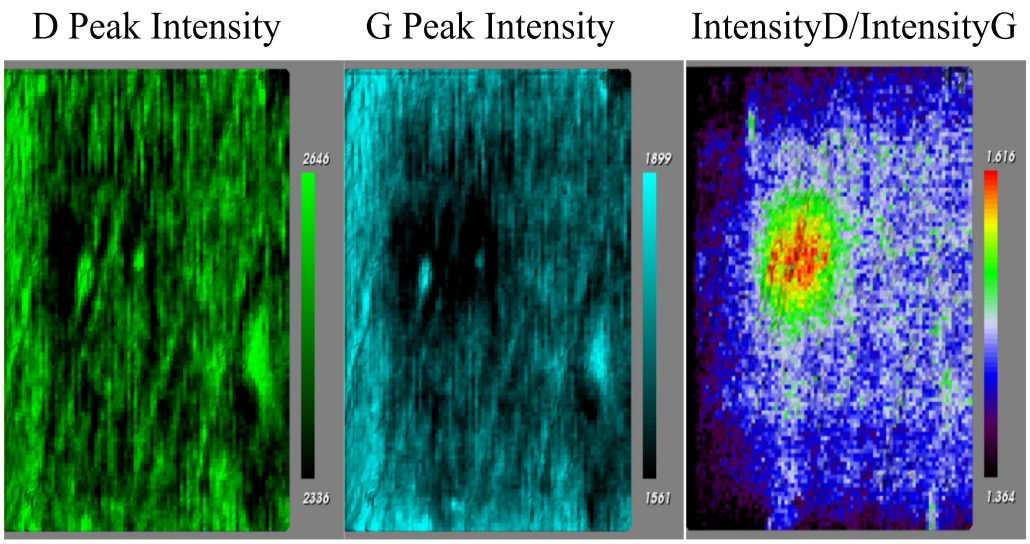

Figure 4.20 D and G peak intensity and ratio.

4.10 XRD Analysis

In HA modified CH membrane, five peaks which belong to HA was detected. These peaks were found at 26.68°, 31.08°, 38.98°, 46.83° and 55.13°. On the other hand, small peak shifts were observed in HA modified CH/GO membrane and HA peaks were found at 26.3°, 31.1°, 41.48°, 48.18° and 53.63°. Specific GO peak was observed at 11.18° and 42.68°. XRD spectrum of membranes can be seen in Figure 4.21 to Figure 4.24.

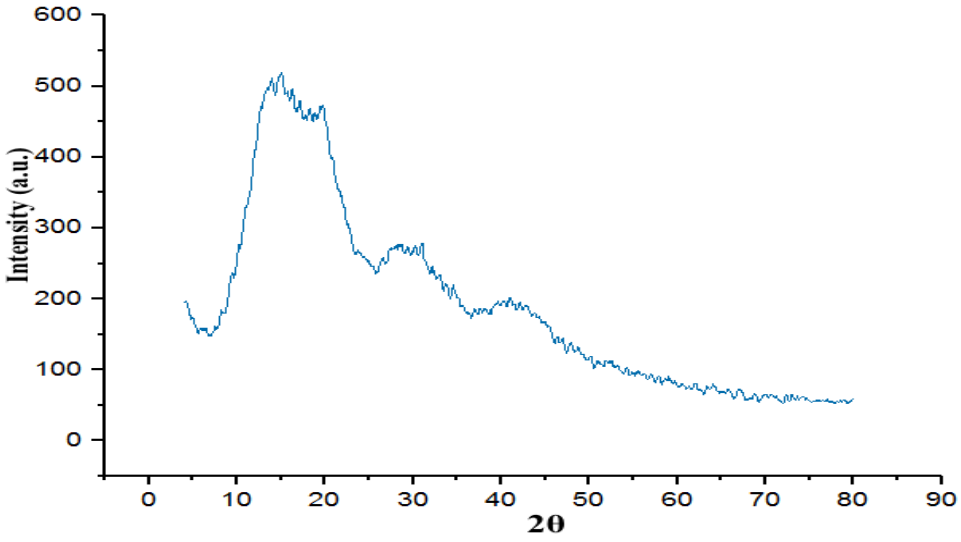

Figure 4.21 XRD spectrum of CH membrane.

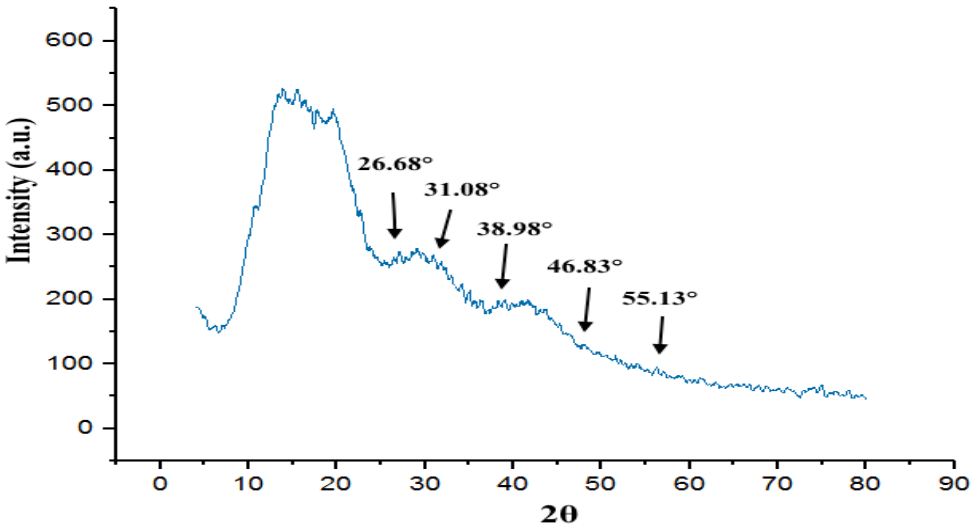

Figure 4.22 XRD spectrum of HA modified CH membrane.

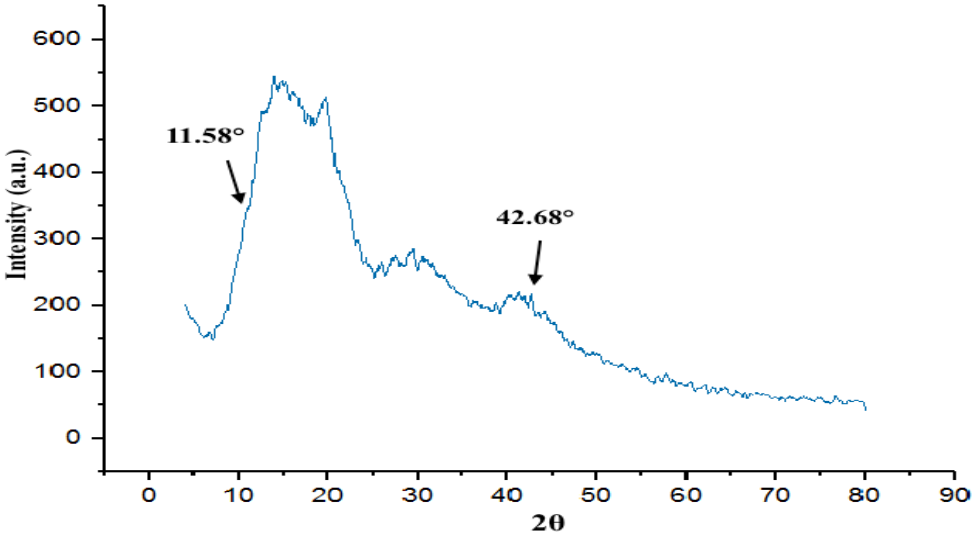

Figure 4.23 XRD spectrum of CH/GO membrane.

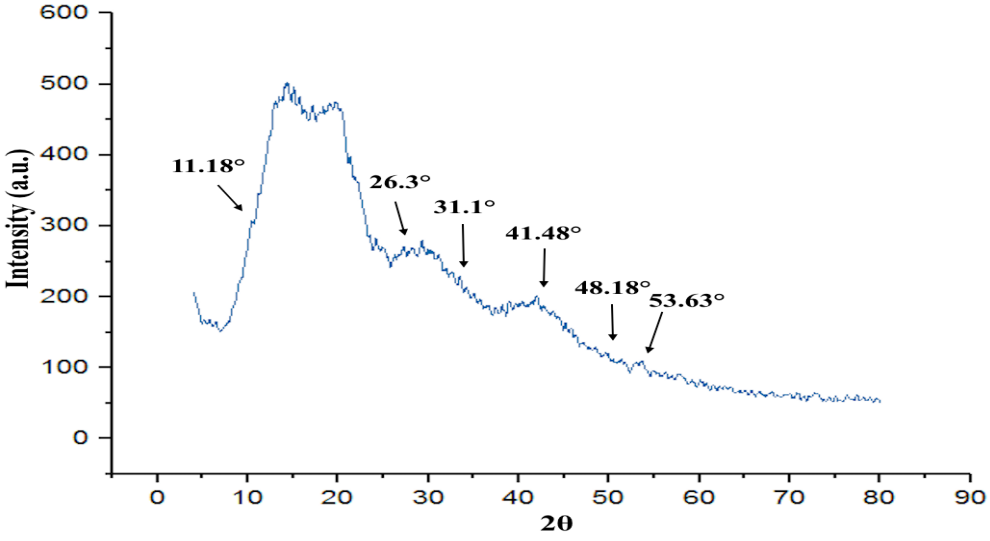

Figure 4.24 XRD spectrum of HA modified CH/GO membrane.

4.11 MTT Assay

MTT assay was used to evaluate viability of hFOB cells over 7 days and absorbance measurement was conducted at 490 nm wavelength. Number of cells were higher at bone surface mimicked membranes at day 1. BSM CH had 123.46%, and HA modified BSM CH/GO membrane had the value of 122.2%. Furthermore, increase in cell number was observed in each membrane at day 4. Highest value was obtained from HA modified BSM CH/GO membrane and HA modified BSM CH, with 132.09%. Bone surface mimicked membranes had better values than plain surfaces when all groups were compared. Most drastic increase was observed between HA modified CH/GO plain and BSM membranes. While the absorbance value of plain HA modified CH/GO was 88.6%, bone surface mimicked membrane had a huge increase and had 132.09%.

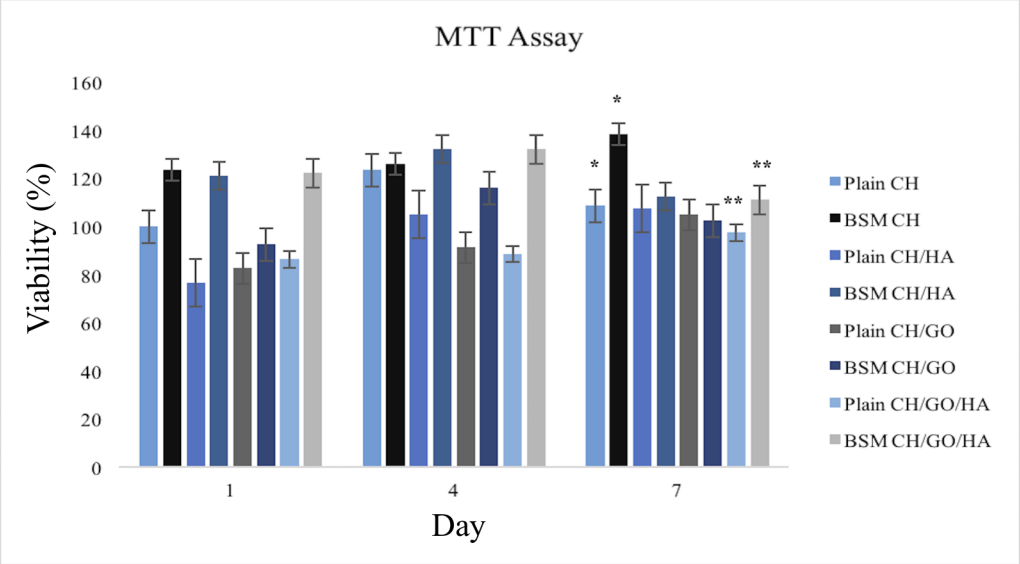

Figure 4.25 Viability of hFOB cells on membranes at day 1,4 and 7.* indicates a significant difference($p<0.01$) between plain CH and BSM CH membranes. ** indicates a significant difference($p<0.01$) between HA modified plain CH/GO and BSM CH/GO membranes at day 7.

At day 7, highest value was gathered from BSM CH membrane. It was followed by BSM HA modified CH and CH/GO membranes with 112.34% and 111.11%. During 7 days, plain membranes demonstrated increase except for plain CH, which decreased from 123.4% to 108.6% at 7. On the other hand, bone surface mimicked membranes showed a different profile. Cell number of bone surface mimicked membranes' increased over 4 days and then it decreased at day 7. Only BSM CH membrane increase over

7 days with 123.45%, 125.92% and 138.27%.Table 4.9 and plain CH membrane was chosen as reference. Figure 4.25 shows comparison of plain and bone surface mimicked membranes.

Table 4.9
Viability at Day 1,4 and 7.

Sample Group	Day 1	Day 4	Day 7
Plain CH	100	123.4	108.6
CH/HA Plain	76.5	104.9	107.4
CH/GO Plain	82.7	91.3	104.9
CH/GO/HA Plain	86.4	88.6	97.5
CH BSM	123.45	125.92	138.27
CH/HA BSM	120.98	132.09	112.34
CH/GO BSM	92.59	116.04	97.5
CH/GO/HA BSM	122.2	132.09	111.11

4.12 hFOB 1.19 Cells SEM Imaging

hFOB cell morphology on different membranes was evaluated by using SEM at day 7. Cells were far from each other on plain chitosan and demonstrated less spreading than other membranes. On CH/GO plain membrane, it was observed that some cells came together and interacted with each other. Furthermore, GO addition had impact on morphology and cells became more spreaded. HA modification of CH and CH/GO membranes resulted to get dense cellular interactions and extensions. Membrane surfaces were fulfilled by osteoblasts. In each membrane type, bone surface mimicking leaded to get more preferable cell morphology. Most intense cellular interaction was observed on bone surface mimicked HA modified CH/GO nanocomposite membranes and cell morphology was like sheet. SEM images with several magnifications, namely 250x, 4000x and 10000x were given in Figure 4.26-Figure 4.28.

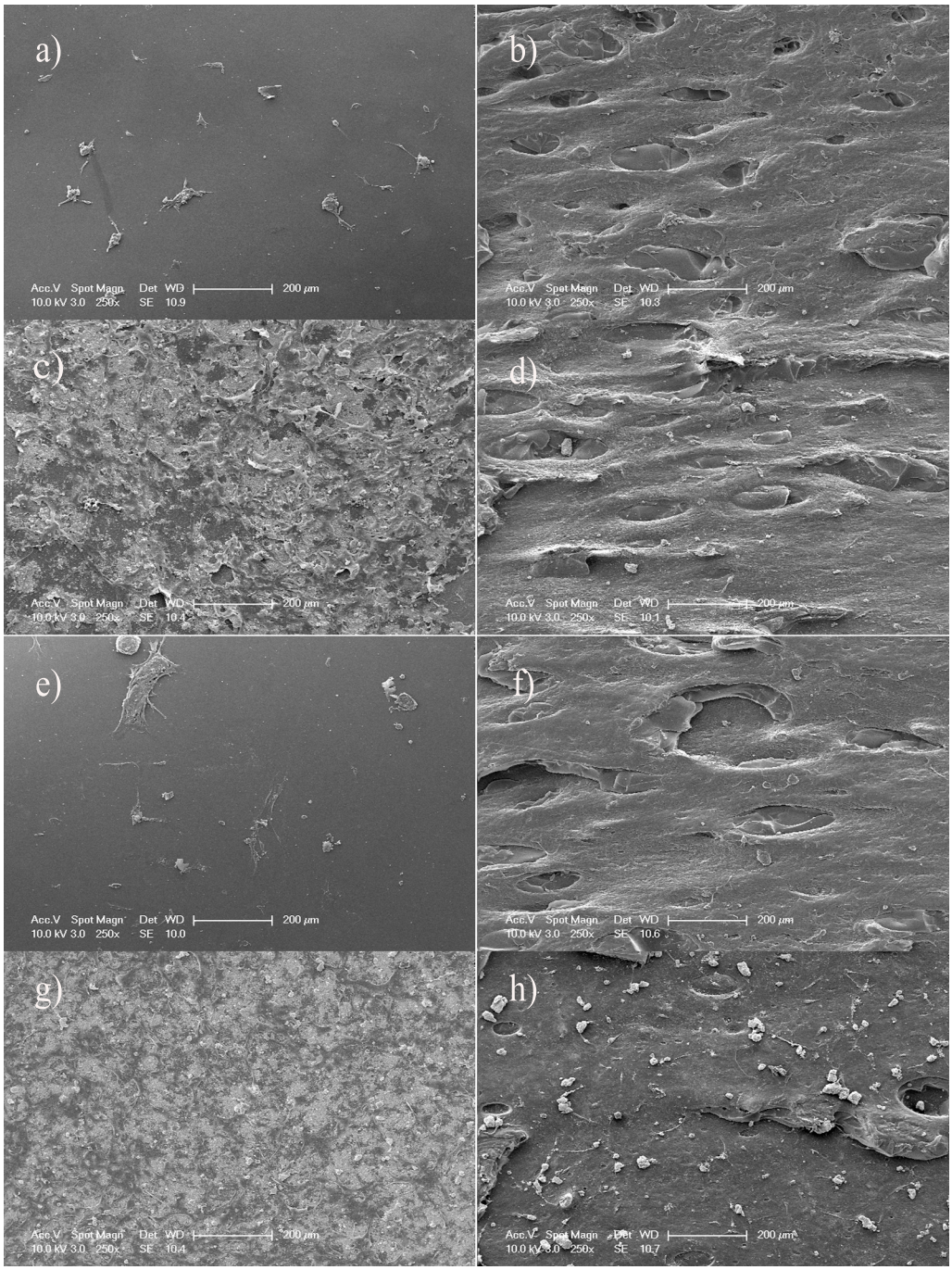

Figure 4.26 250x magnified SEM images of hFOB 1.19 cells at day 7 a) CH plain b) CH BSM c) CH/HA plain d) CH/HA BSM e) CH/GO plain f) CH/GO BSM g) CH/GO/HA plain h) CH/GO/HA BSM.

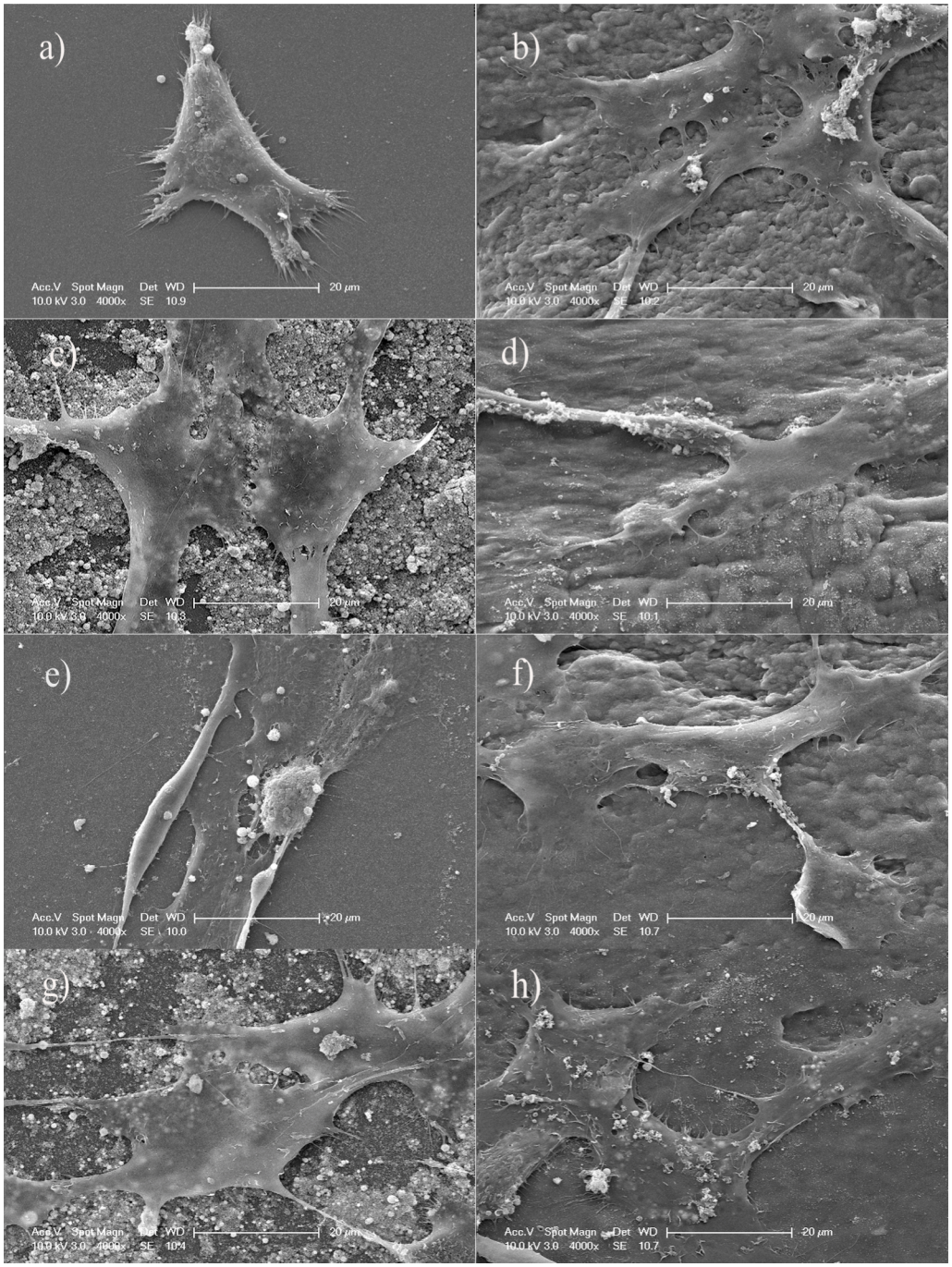

Figure 4.27 4000x magnified SEM images of hFOB 1.19 cells at day 7 a) CH plain b) CH BSM c) CH/HA plain d) CH/HA BSM e) CH/GO plain f) CH/GO BSM g) CH/GO/HA plain h) CH/GO/HA BSM.

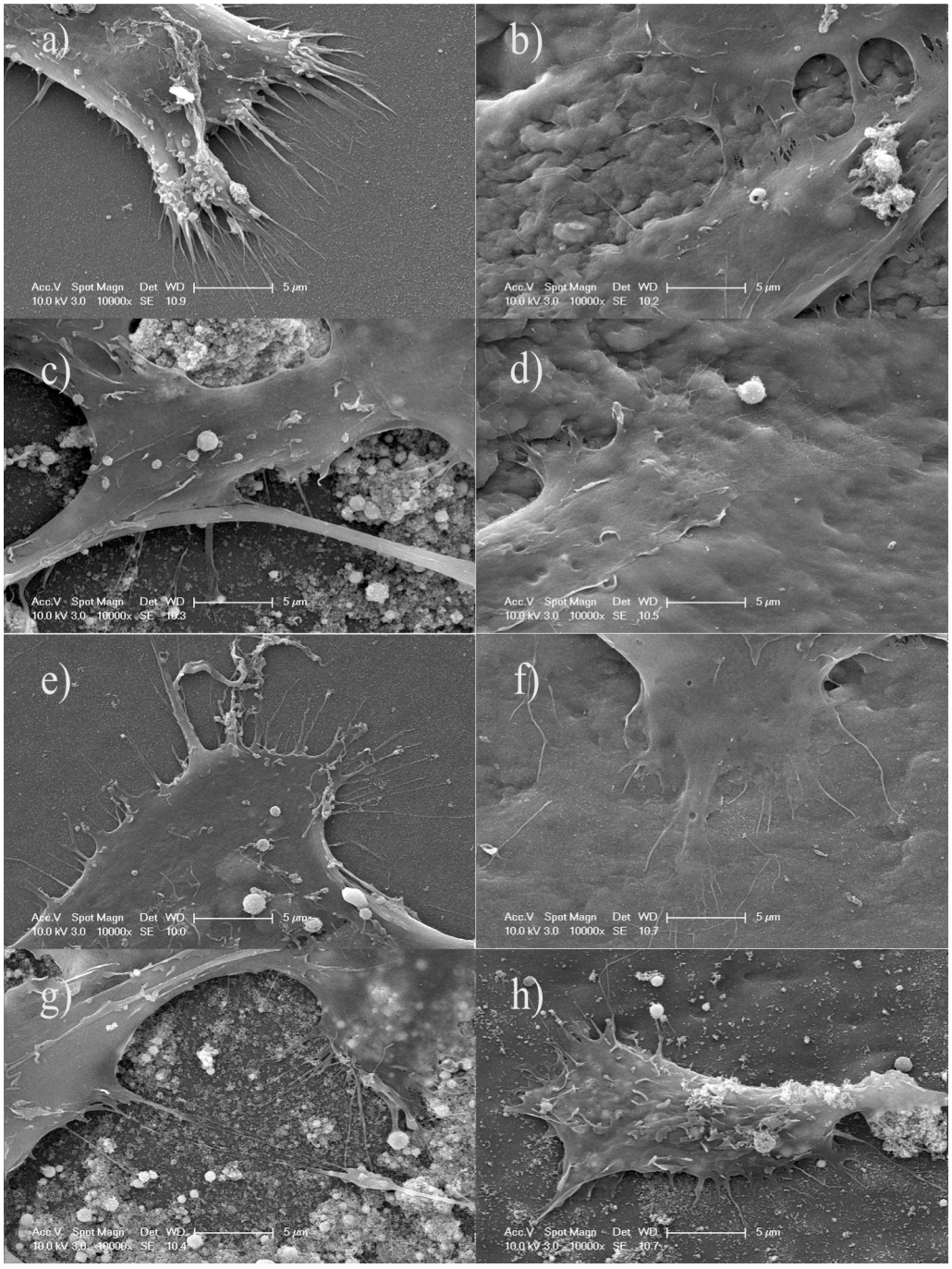

Figure 4.28 10000x magnified SEM images of hFOB 1.19 cells at day 7 a) CH plain b) CH BSM c) CH/HA plain d) CH/HA BSM e) CH/GO plain f) CH/GO BSM g) CH/GO/HA plain h) CH/GO/HA BSM.

5. DISCUSSION

Topographical characterization of mimicked surfaces was performed by using SEM and confocal microscopy imaging. Both imaging techniques demonstrated that CH and CH/GO based membrane topography contains similar structures with bone surface and indicates mimicking procedure was successful. On the other hand, size of microstructures had few changes in mimicked membranes because of elasticity of polymeric nature of preferred main material. Furthermore, some residues of PDMS were observed at 1000x and 5000x magnified SEM images and it was also concluded that sticky nature of PDMS had slight impact on bone surface mimicking.

Bone surface is an heterogeonous surface and has a rough surface that consists of micro and nanostructures. Confocal microscopy was used to understand roughness value differences of plain and mimicked membranes. While plain CH had nano-sized roughness value that was 56.992 nm, bone surface mimicked CH membrane had micrometer roughness, which was 5.245 μm. The dramatic increase in roughness value indicated that fabricated mimicked surfaces were eligible to copy bone surface, successfully. In addition to this, BSM CH had a heterogeneonous surface profile, which indicates similarity with bone surface. When Sp and Sv values were considered, it was observed that maximum peak height was 26.988 μm and the maximum valley depth was 38.910 μm. Negative value of Ssk parameter demonstrated that mimicked surface area was dominated by valleys.

Water absorption is an important phenomenon for in vivo applications since implanted material interacts with body fluidics and swelling capacity of biomaterial should be tested before applications. In this thesis, bone surface mimicking and GO addition influence on swelling capacity was analyzed. When the results were evaluated, it was observed that bone surface mimicking had significantly positive impact on swelling capacity of the membranes. Bone surface mimicked membranes demonstrated better swelling in each comparison. SEM and confocal microscopy images showed that

bone surface has extremely rough surface and it can be concluded that mimicking microstructures on bone surface is quite effective to increase swelling capacity of scaffolds.

Furthermore, GO is a hydrophilic material and contact angle value of it's was reported between 30-60°,which consist of oxygen groups in it's structure and able to behave like a cross-linker. Also, wetting and swelling properties of GO can be tuned with altering oxidization degree [54]. In our experiment, addition of GO was beneficial to increase swelling capacity of the plain membranes. GO added plain membranes showed higher absorption of PBS, which means that GO acts like a cross-linker and helps to absorb more liquid in the structure of chitosan. In the literature, there were some reports, which have investigated the swelling ratio relationship of CH and GO. In swelling process, amino groups of CH are protonated and it leads to polymer chain relaxation which increases swelling ratio. When CH and GO come together, the amino groups of CH interact with hydroxyl groups of GO. If there is a dense interaction of these groups, it is possible to observe decrease in swelling ratio [55]. When BSM CH and BSM CH/GO was compared, there was a slight decrease in swelling capacity of BSM CH/GO. The reason might be the roughness of bone surface structure, which may lead to unfolding of GO sheets that causes dense interaction with CH. During casting and drying process of bone surface mimicked membranes, aggregation of GO sheets might have occurred and leaded o loss of homogeneity, which caused to decrease in flexibility of polymer chains.

In addition to water absorption, wettability properties of membranes were assessed by water contact angle measurements. CH is a hydrogel, which is able to absorb water and faces with deformations in the structure during absorption. The structure becomes more swollen and contact angle value changes within time, as well. For instance, water contact angle of plain CH membrane decreased from 88.99° to 74.52° during 10 minutes.

Because of this phenomena, contact angle measurement was conducted during 10 minutes. In literature, water contact angle of graphene is reported between 87-127° [56]. GO has better wettability because of having oxide groups in structure and contact

angle value is reported between 30-60°. Oxidization ratio and method leads to change in contact angle value [54]. On the other hand, water contact angle value of CH was reported as 88.4° [57].

According to Wenzel theory, surface roughness increases wetting property if material is hydrophilic [58]. When plain CH and BSM CH groups are compared, we observed that such microstructures are very effective to get lower contact angle and good wettability. BSM CH showed more hydrophilic character with rougher surface, which leads to augmentation of the surface area. On the other hand, it was observed that plain CH/GO had the lowest contact angle value with 63.95°, which showed better wettability. The reason might be that GO is a highly hydrophilic material and longer interaction of droplet increases GO interaction which behaves like cross-linker and helps to get more hydrophilic structure [59]. In contrast, BSM CH/GO had the highest contact angle, which means it is less hydrophilic. The reason of such a huge difference might be the loss of homogeneity during casting process, since bone surface has depths and peaks. Aggregation of GO flakes might cause less interaction of oxide groups and droplet.

In addition to physical characterizations, chemical characterization techniques were conducted to understand chemical structures and interactions between membrane components. First of all, FT-IR spectroscopy analysis was performed to optimize time parameter for HA modification. In the literature, it was reported that specific CH bands are found at 3352 cm^{-1} that belongs to -OH and -CH_3. Also, N-H bending vibration and -OH vibrations are observed at 1560 and 1404 cm^{-1}, respectively. 1320 and 1077 cm^{-1} bands are attributed to C-O-N and C-O stretching. C=O stretching band is found at 1650 cm^{-1}. Free acetic acid can be identified with specific band, which is located at 1706 cm^{-1} [60]. For confirming of HA modification, specific phosphate groups of HA can be detected between 900-1100 cm^{-1} and 500-600 cm^{-1} bands [48].

In this thesis, the bands which are attributed to CH were observed at 3355 cm^{-1} for -OH and -CH_3 groups. N-H bending vibration and -OH vibrations were observed at 1586 cm^{-1} and 1417 cm^{-1}, respectively. 1374 cm^{-1} bands were attributed to C-O-N

and also C=O stretching band was found at 1646 cm^{-1}. The band of 1706 cm^{-1} was not observed and it was concluded that free acetic acid groups were successfully neutralized with NaOH treatment. Furthermore, specific peaks which belong to HA phosphate groups was observed at 1027, 603 and 570 cm^{-1}. When transmittance change was considered after surface modification, 5 minutes UV/Ozone treatment was the most efficient time parameter, but it leaded defects on membranes' surfaces as a result of high energy application. With considering surface defects that were observed by SEM imaging, we decided to continue with 2 minutes UV/Ozone treatment, which provides efficient amount of modification and didn't lead any surface defects. Moreover, SEM imaging was used to visualize HA nanoparticle distribution on modified membranes and non-uniform distribution of the nanoparticles was observed.

Atomic composition of membranes was analyzed by XPS spectrum. CH chemical structure gives three major peaks which attribute to O1s, N1s and C1s. Furthermore, HA forms Ca2s, Ca2p, P2s and P2p specific peaks and GO only shows C1s and O1s peaks [52][61]. Calcium phosphate ratio is an important factor for bone tissue engineering applications and natural bone has 1.67 Ca2p/P2p ratio which is a reference [53]. Ca2p/P2p ratio of pure HA, HA modified CH and HA modified CH/GO was calculated as 1.5, 1.29 and 1.39 were measured after XPS analysis of fabricated membranes, respectively.

After XPS analysis of fabricated membranes, specific peaks of CH that are O1s at 532.08 eV, N1s at 395.08 eV and C1s at 284.08 eV were observed. On the other hand, GO addition resulted changes in elemental composition ratio. O1s ratio increased with the addition of GO since it contains high amount of oxygen groups in it's chemical structure. Success of HA modification was confirmed via gathering calcium and phosphate peaks, again. Ca2s and Ca2p peaks were detected at 436.08 and 346.08 eV, respectively. Moreover, P2s peak was observed at 188.08 eV, while P2p was at 134.08 eV.

X-Ray diffraction analysis was conducted to identify existence of crystal structures. In literature, it was mentioned that hydroxyapatite shows peaks 25.9°, 31.8°,

39.8°, 46.7°, 49.5° and 53.2°. CH shows peaks around 10° and 20°, and also GO has a sharp peak at 11.1° [62]. In this thesis, peaks at 26.68°, 31.08°, 38.98°, 46.83° and 55.13° were found in HA modified CH membrane. It can be approved that nanocrystal structured HA, which is osseointegrative, was assembled with CH membrane.For HA modified CH/GO membrane,peaks of HA were found at 26.3°, 31.1°, 41.48°, 48.18° and 53.63° and it was concluded that GO addition resulted some shifts when it interacts with CH and HA. GO peaks were observed at 11.18° and 42.68°.

Chemical composition and molecular interactions inside the membranes were analyzed with the help of Raman spectroscopy. Furthermore, GO existence and also conformation was evaluated by D and G peak detection and intensity distribution. 3 different phosphate (PO_4^{-3}) groups of HA were detected in CH and CH/GO based membranes and it indicated that membrane surfaces were surrounded by HA residues. In the structure of HA modified CH/GO membranes, C-H out of plane deformation, which belongs to CH structure was observed and intensity of peak decreased after GO interaction. The D and G band of GO helps to understand disorders in structure. The D band indicates disorders in aromatic structure, while the G band shows in-plane vibration of sp^2 carbons [62]. It was reported that pure GO has 1.1 I_D/I_G and the ratio goes up with the increase of disordered flakes [62]. In our thesis, shifts of D and G bands were observed after CH and HA interaction and it can be concluded that increase in structure disorder is available. Intensity ratio of D and G bands were analyzed to understand structure disorder of GO and I_D/I_G value was calculated as the range of 1.364 and 1.616. When this ratio was compared with pure GO value, which was obtained from literature, it can be concluded that CH and HA interaction resulted to get disordered structure of GO.

MTT assay was conducted at day 1,4 and 7 to evaluate cell viability on the fabricated membranes. First of all, it can be said that bone surface mimicked membranes were more efficient than plain membranes as increased cell viability. At day 1, bone surface mimicking had leaded to significant enhance of cell number. BSM CH membrane had 123.45%, while plain had the value of 100%. Bone surface mimicking increased value of HA modified CH membrane to 120.98% when plain membrane was

76.5%. HA modified BSM CH/GO had 122.2%, which was the highest value after BSM CH membrane. The cell number had increased in each membrane at day 4. The highest value was obtained from HA modified BSM CH and HA modified BSM CH/GO with 132.09%. At day 7, number of cells decreased in BSM membranes except for BSM CH. On the other hand, plain surfaces continued to go up. BSM CH membrane was the best group with 138.27%, which was followed with HA modified BSM CH and CH/GO. Bone surface mimicked membranes except for BSM CH/GO performed better effect on cells.

SEM images of hFOB cells at day 7 was captured to evaluate cell morphology and 250x, 4000x and 10000x magnified images were used for this aim. On plain CH, it was observed that cells had located far from each others and interactions between cells were limited. On the other hand, filopodia and lamellipodia extensions were observed. GO added CH plain membrane leaded to get more spreaded cell morphology and some of cells started to league together. Longer extension of filopodia and lamellipodia were observed. It can be said that GO helps to get better cell spreading. Cells which are seeded on HA modified plain chitosan membrane demonstrated enormous interaction of cells and spreading. The surface of material was covered with the cells and direct contact between cells with using their extensions were observed. On the other hand, HA modified CH/GO plain membrane had resulted more cell spreading and greater filopodia and lamellipodia extensions, when it is compared with HA modified plain CH membrane in this study. In the literature, it was confirmed that combination of CH, GO and HA had resulted to get spreaded cell morphology [63].

Usage of CH, GO and HA based biomaterials in bone tissue engineering is very popular and preferred because of unique properties. On the other hand, several studies have been conducted to mimic bone surface topography and interpret cell behavior on the topography. In literature, there is no study that combines both of two approaches found and combination of two approaches was evaluated for the first time in this thesis.

Schwartz et al. demonstrated that osteoblasts are affected by surface roughness and focal attachments causes changes in cell morphology [64]. Palin et al. used PLGA

polymer to mimic nanofeatures of bone surface and human osteoblasts were seeded on mimicked surface. They observed that mimicked surface enhanced osteoblast adhesion and proliferation [6]. Shi et al. fabricated nanosheets that are able to mimic bone surface structures. PLGA nanosheets were fabricated and human adipose-derived mesenchymal stem cells (ADMSCs) were used in this study. It was reported that surface structures promoted osteogenic marker expression and cell alignment was controlled by surface structures [5]. Depan et al. worked on CH/GO plain membranes and demonstrated that MC3T3-E1 pre-osteoblast cell attachment and proliferation increased with GO addition [65]. In addition to this, they worked on HA biomineralization of CH/GO composite plain membranes by using MC3T3-E1 pre-osteoblast cells. They concluded that combination of these three biomaterials had more effective results on cell attachment and proliferation [63]. Li et al. worked on CH-GO-HA nanocomposites with human osteoblast-like(MG-63) cells and synergetic effect on cell attachment were observed. Furthermore, they concluded that GO enhances alkaline phosphatese activity [62]. Yang et al. designed CH/GO/HA composite hydrogels and rat mesenchymal stem cells (rBMSCs) were used for cell culture study. They demonstrated that composite hydrogel improved cell attachment when it is compared with pure HA. On the other hand, cell viability of composite was nearly same with HA [66].

In addition to chemical alterations of membranes, surface topography had impact on regulation of cell morphology and cell viability. According to MTT assay results, bone surface mimicking had positive impact on cell viability. BSM CH membrane showed the highest viability value with 138.42% and HA modified CH and CH/GO membranes followed it with 112.34% and 111.11%, respectively. In addition to viability, cell spreading was better on bone surface mimicked membranes and the cells could consider that they were in their natural niche. HA modified bone surface mimicked CH/GO membrane showed the best cellular interactions and morphology. As a conclusion, when all groups were considered, bone surface mimicked HA modified CH/GO membrane had better results in terms of cell spreading. It can be interpreted that bone surface topography is quite beneficial to get better cell spreading and viability. HA modification and GO addition with bone surface mimicking is very useful to obtain preferred cell morphology and also provides good viability.

REFERENCES

1. Feng, X., and J. M. McDonald, "Disorders of bone remodeling.," *Annual review of pathology*, Vol. 6, pp. 121–45, 2011.

2. Fernandez-Yague, M. A., S. A. Abbah, L. McNamara, D. I. Zeugolis, A. Pandit, and M. J. Biggs, "Biomimetic approaches in bone tissue engineering: integrating biological and physicomechanical strategies," *Advanced drug delivery reviews*, Vol. 84, pp. 1–29, 2015.

3. Ma, P. X., "Biomimetic materials for tissue engineering," *Advanced drug delivery reviews*, Vol. 60, no. 2, pp. 184–198, 2008.

4. Boyan, B. D., T. W. Hummert, D. D. Dean, and Z. Schwartz, "Role of material surfaces in regulating bone and cartilage cell response," *Biomaterials*, Vol. 17, no. 2, pp. 137–146, 1996.

5. Shi, X., T. Fujie, A. Saito, S. Takeoka, Y. Hou, Y. Shu, M. Chen, H. Wu, and A. Khademhosseini, "Periosteum-mimetic structures made from freestanding microgrooved nanosheets," *Advanced Materials*, Vol. 26, no. 20, pp. 3290–3296, 2014.

6. Palin, E., H. Liu, and T. J. Webster, "Mimicking the nanofeatures of bone increases bone-forming cell adhesion and proliferation," *Nanotechnology*, Vol. 16, no. 9, p. 1828, 2005.

7. Logithkumar, R., A. Keshavnarayan, S. Dhivya, A. Chawla, S. Saravanan, and N. Selvamurugan, "A review of chitosan and its derivatives in bone tissue engineering," 2016.

8. Motamedian, S. R., S. Hosseinpour, M. G. Ahsaie, and A. Khojasteh, "Smart scaffolds in bone tissue engineering: A systematic review of literature.," *World journal of stem cells*, Vol. 7, no. 3, pp. 657–68, 2015.

9. Goenka, S., V. Sant, and S. Sant, "Graphene-based nanomaterials for drug delivery and tissue engineering," 2014.

10. Olszta, M. J., X. Cheng, S. S. Jee, R. Kumar, Y. Y. Kim, M. J. Kaufman, E. P. Douglas, and L. B. Gower, "Bone structure and formation: A new perspective," 2007.

11. Kanczler, J. M., and R. O. C. Oreffo, "Osteogenesis and angiogenesis: The potential for engineering bone," 2008.

12. Wenger, D. R., *Textbook of Disorders and Injuries of the Musculoskeletal System,*, Vol. 20, 2000.

13. Kini, U., and B. N. Nandeesh, "Physiology of bone formation, remodeling, and metabolism," in *Radionuclide and Hybrid Bone Imaging*, Vol. 9783642024, pp. 29–57, 2012.

14. Dimitriou, R., E. Jones, D. McGonagle, and P. V. Giannoudis, "Bone regeneration: current concepts and future directions.," *BMC medicine*, Vol. 9, p. 66, 2011.

15. Porter, J. R., T. T. Ruckh, and K. C. Popat, "Bone tissue engineering: A review in bone biomimetics and drug delivery strategies," *Biotechnology Progress*, Vol. 25, no. 6, pp. 1539–1560, 2009.

16. Orr, A. W., B. P. Helmke, B. R. Blackman, and M. A. Schwartz, "Mechanisms of mechanotransduction," 2006.

17. Lu, Z., S. I. Roohani-Esfahani, G. Wang, and H. Zreiqat, "Bone biomimetic microenvironment induces osteogenic differentiation of adipose tissue-derived mesenchymal stem cells," *Nanomedicine: Nanotechnology, Biology, and Medicine*, Vol. 8, no. 4, pp. 507–515, 2012.

18. Xia, Y., and G. M. Whitesides, "Soft Lithography," *Annual Review of Materials Science*, Vol. 28, no. 1, pp. 153–184, 1998.

19. Whitesides, G. M., E. Ostuni, S. Takayama, X. Jiang, and D. E. Ingber, "Soft lithography in biology and biochemistry.," *Annual review of biomedical engineering*, Vol. 3, pp. 335–73, 2001.

20. Dai, S., D. Zhang, Q. Shi, X. Han, S. Wang, and Z. Du, "Biomimetic fabrication and tunable wetting properties of three-dimensional hierarchical zno structures by combining soft lithography templated with lotus leaf and hydrothermal treatments," *CrystEngComm*, Vol. 15, no. 27, pp. 5417–5424, 2013.

21. Gao, X., X. Yan, X. Yao, L. Xu, K. Zhang, J. Zhang, B. Yang, and L. Jiang, "The dry-style antifogging properties of mosquito compound eyes and artificial analogues prepared by soft lithography," *Advanced Materials*, Vol. 19, no. 17, pp. 2213–2217, 2007.

22. Auzelyte, V., V. Flauraud, V. J. Cadarso, T. Kiefer, and J. Brugger, "Biomimetic soft lithography on curved nanostructured surfaces," *Microelectronic Engineering*, Vol. 97, pp. 269–271, 2012.

23. Yuan, H., and K. de Groot, "Calcium phosphate biomaterials: an overview," in *Learning from Nature How to Design New Implantable Biomaterialsis: From Biomineralization Fundamentals to Biomimetic Materials and Processing Routes*, pp. 37–57, Springer, 2004.

24. Amini, A. R., C. T. Laurencin, and S. P. Nukavarapu, "Bone tissue engineering: recent advances and challenges.," *Critical reviews in biomedical engineering*, Vol. 40, no. 5, pp. 363–408, 2012.

25. Park, J. B., "The use of hydrogels in bone-tissue engineering," 2011.

26. Sabir, M. I., X. Xu, and L. Li, "A review on biodegradable polymeric materials for bone tissue engineering applications," *Journal of Materials Science*, Vol. 44, no. 21, pp. 5713–5724, 2009.

27. Kroeze, R. J., M. N. Helder, L. E. Govaert, and T. H. Smit, "Biodegradable polymers in bone tissue engineering," *Materials*, Vol. 2, no. 3, pp. 833–856, 2009.

28. Ramasamy, T., T. H. Tran, H. J. Cho, J. H. Kim, Y. I. Kim, J. Y. Jeon, H.-G. Choi, C. S. Yong, and J. O. Kim, "Chitosan-based polyelectrolyte complexes as potential nanoparticulate carriers: physicochemical and biological characterization," *Pharmaceutical research*, Vol. 31, no. 5, pp. 1302–1314, 2014.

29. Pillai, C., W. Paul, and C. P. Sharma, "Chitin and chitosan polymers: Chemistry, solubility and fiber formation," *Progress in polymer science*, Vol. 34, no. 7, pp. 641–678, 2009.

30. Hoctor, E., J. Killion, D. Devine, L. Geever, C. Higginbotham, D. Road, C. Westmeath, B. Israel, and D. Medical, "The Preparation Of Nanocomposite Scaffolds For Use In Bone Tissue Engineering," *Australian Journal of Basic and Applied Sciences*, Vol. 7, no. 5, pp. 140–149, 2013.

31. Thein-Han, W. W., and R. D. K. Misra, "Biomimetic chitosan-nanohydroxyapatite composite scaffolds for bone tissue engineering," *Acta Biomaterialia*, Vol. 5, no. 4, pp. 1182–1197, 2009.

32. Ge, Z., S. Baguenard, L. Y. Lim, A. Wee, and E. Khor, "Hydroxyapatite–chitin materials as potential tissue engineered bone substitutes," *Biomaterials*, Vol. 25, no. 6, pp. 1049–1058, 2004.

33. Zhou, H., and J. Lee, "Nanoscale hydroxyapatite particles for bone tissue engineering," *Acta biomaterialia*, Vol. 7, no. 7, pp. 2769–2781, 2011.

34. Iannazzo, D., *Drug Delivery Strategies for Bone Tissue Regeneration*, Omics, 2015.

35. Gong, T., J. Xie, J. Liao, T. Zhang, S. Lin, and Y. Lin, "Nanomaterials and bone regeneration.," *Bone research*, Vol. 3, no. August, p. 15029, 2015.

36. Kong, L., Y. Gao, G. Lu, Y. Gong, N. Zhao, and X. Zhang, "A study on the bioactivity of chitosan/nano-hydroxyapatite composite scaffolds for bone tissue engineering," *European Polymer Journal*, Vol. 42, no. 12, pp. 3171–3179, 2006.

37. Chen, Y., L. Chen, H. Bai, and L. Li, "Graphene oxide–chitosan composite hydrogels as broad-spectrum adsorbents for water purification," *Journal of Materials Chemistry A*, Vol. 1, no. 6, p. 1992, 2013.

38. Gu, M., Y. Liu, T. Chen, F. Du, X. Zhao, C. Xiong, and Y. Zhou, "Is graphene a promising nano-material for promoting surface modification of implants or scaffold materials in bone tissue engineering?," *Tissue Engineering Part B: Reviews*, Vol. 20, no. 5, pp. 477–491, 2014.

39. Nayak, T. R., H. Andersen, V. S. Makam, C. Khaw, S. Bae, X. Xu, P.-L. R. Ee, J.-H. Ahn, B. H. Hong, G. Pastorin, *et al.*, "Graphene for controlled and accelerated osteogenic differentiation of human mesenchymal stem cells," *ACS nano*, Vol. 5, no. 6, pp. 4670–4678, 2011.

40. Kalbacova, M., A. Broz, J. Kong, and M. Kalbac, "Graphene substrates promote adherence of human osteoblasts and mesenchymal stromal cells," *Carbon*, Vol. 48, no. 15, pp. 4323–4329, 2010.

41. Dinescu, S., M. Ionita, A. M. Pandele, B. Galateanu, H. Iovu, A. Ardelean, M. Costache, and A. Hermenean, "In vitro cytocompatibility evaluation of chitosan/graphene oxide 3d scaffold composites designed for bone tissue engineering," *Bio-medical materials and engineering*, Vol. 24, no. 6, pp. 2249–2256, 2014.

42. Demir, O., "Bone surface mimicked biodegradable polymeric scaffolds," Master's thesis, Bogazici University, 2014.

43. Rostami, S., "Fabrication and characterization of sharkskin mimicked chitosan-graphene oxide nanocomposite membranes," Master's thesis, Bogazici University, 2016.

44. Noriega, S. E., and A. Subramanian, "Consequences of neutralization on the proliferation and cytoskeletal organization of chondrocytes on chitosan-based matrices," *International Journal of Carbohydrate Chemistry*, Vol. 2011, 2011.

45. Zuo, P.-P., H.-F. Feng, Z.-Z. Xu, L.-F. Zhang, Y.-L. Zhang, W. Xia, and W.-Q. Zhang, "Fabrication of biocompatible and mechanically reinforced graphene oxide-chitosan nanocomposite films," *Chemistry Central Journal*, Vol. 7, no. 1, p. 1, 2013.

46. Dal Pozzo, A., L. Vanini, M. Fagnoni, M. Guerrini, A. De Benedittis, and R. Muzzarelli, "Preparation and characterization of poly (ethylene glycol)-crosslinked reacetylated chitosans," *Carbohydrate Polymers*, Vol. 42, no. 2, pp. 201–206, 2000.

47. Yanagida, H., M. Okada, M. Masuda, M. Ueki, I. Narama, S. Kitao, Y. Koyama, T. Furuzono, and K. Takakuda, "Cell adhesion and tissue response to hydroxyapatite nanocrystal-coated poly (l-lactic acid) fabric," *Journal of bioscience and bioengineering*, Vol. 108, no. 3, pp. 235–243, 2009.

48. Frohbergh, M. E., A. Katsman, G. P. Botta, P. Lazarovici, C. L. Schauer, U. G. Wegst, and P. I. Lelkes, "Electrospun hydroxyapatite-containing chitosan nanofibers crosslinked with genipin for bone tissue engineering," *Biomaterials*, Vol. 33, no. 36, pp. 9167–9178, 2012.

49. Chen, J.-P., S.-H. Chen, and G.-J. Lai, "Preparation and characterization of biomimetic silk fibroin/chitosan composite nanofibers by electrospinning for osteoblasts culture," *Nanoscale research letters*, Vol. 7, no. 1, p. 1, 2012.

50. Gupta, S. K., A. K. Dinda, P. D. Potdar, and N. C. Mishra, "Modification of decellularized goat-lung scaffold with chitosan/nanohydroxyapatite composite for bone tissue engineering applications," *BioMed research international*, Vol. 2013, 2013.

51. Boccaccini, A., *Ceramics for Environmental and Energy Applications*, Wiley.

52. Maachou, H., M. J. Genet, D. Aliouche, C. C. Dupont-Gillain, and P. G. Rouxhet, "Xps analysis of chitosan–hydroxyapatite biomaterials: from elements to compounds," *Surface and Interface Analysis*, Vol. 45, no. 7, pp. 1088–1097, 2013.

53. Zhang, Y., J. R. Venugopal, A. El-Turki, S. Ramakrishna, B. Su, and C. T. Lim, "Electrospun biomimetic nanocomposite nanofibers of hydroxyapatite/chitosan for bone tissue engineering," *Biomaterials*, Vol. 29, no. 32, pp. 4314–4322, 2008.

54. Wei, N., C. Lv, and Z. Xu, "Wetting of graphene oxide: A molecular dynamics study," *Langmuir*, Vol. 30, no. 12, pp. 3572–3578, 2014.

55. Li, J., N. Ren, J. Qiu, X. Mou, and H. Liu, "Graphene oxide-reinforced biodegradable genipin-cross-linked chitosan fluorescent biocomposite film and its cytocompatibility," *International journal of nanomedicine*, Vol. 8, p. 3415, 2013.

56. Taherian, F., V. Marcon, N. F. van der Vegt, and F. Leroy, "What is the contact angle of water on graphene?," *Langmuir*, Vol. 29, no. 5, pp. 1457–1465, 2013.

57. Rivero, S., M. García, and A. Pinotti, "Physical and chemical treatments on chitosan matrix to modify film properties and kinetics of biodegradation," *Journal of Materials Physics and Chemistry*, Vol. 1, no. 3, pp. 51–57, 2013.

58. Wenzel, R. N., "Resistance of solid surfaces to wetting by water," *Industrial & Engineering Chemistry*, Vol. 28, no. 8, pp. 988–994, 1936.

59. Shao, L., X. Chang, Y. Zhang, Y. Huang, Y. Yao, and Z. Guo, "Graphene oxide cross-linked chitosan nanocomposite membrane," *Applied Surface Science*, Vol. 280, pp. 989–992, 2013.

60. Fernandes, L. L., C. X. Resende, D. S. Tavares, G. A. Soares, L. O. Castro, and J. M. Granjeiro, "Cytocompatibility of chitosan and collagen-chitosan scaffolds for tissue engineering," *Polimeros*, Vol. 21, no. 1, pp. 1–6, 2011.

61. Jung, M.-H., M. G. Kang, and M.-J. Chu, "Iodide-functionalized graphene electrolyte for highly efficient dye-sensitized solar cells," *Journal of Materials Chemistry*, Vol. 22, no. 32, pp. 16477–16483, 2012.

62. Li, M., Y. Wang, Q. Liu, Q. Li, Y. Cheng, Y. Zheng, T. Xi, and S. Wei, "In situ synthesis and biocompatibility of nano hydroxyapatite on pristine and chitosan functionalized graphene oxide," *Journal of Materials Chemistry B*, Vol. 1, no. 4, pp. 475–484, 2013.

63. Depan, D., T. Pesacreta, and R. Misra, "The synergistic effect of a hybrid graphene oxide–chitosan system and biomimetic mineralization on osteoblast functions," *Biomaterials Science*, Vol. 2, no. 2, pp. 264–274, 2014.

64. Boyan, B. D., T. W. Hummert, D. D. Dean, and Z. Schwartz, "Role of material surfaces in regulating bone and cartilage cell response," *Biomaterials*, Vol. 17, no. 2, pp. 137–146, 1996.

65. Depan, D., B. Girase, J. Shah, and R. Misra, "Structure–process–property relationship of the polar graphene oxide-mediated cellular response and stimulated growth of osteoblasts on hybrid chitosan network structure nanocomposite scaffolds," *Acta biomaterialia*, Vol. 7, no. 9, pp. 3432–3445, 2011.

66. Yu, P., R.-Y. Bao, X.-J. Shi, W. Yang, and M.-B. Yang, "Self-assembled high-strength hydroxyapatite/graphene oxide/chitosan composite hydrogel for bone tissue engineering," *Carbohydrate Polymers*, Vol. 155, pp. 507–515, 2017.